THE UNIVERSITY OF CHICAGO

ENGINEERING LOV2 FOR THE CONTROL AND STUDY OF MOTOR PROTEINS

A DISSERTATION SUBMITTED TO

THE FACULTY OF THE DIVISION OF THE BIOLOGICAL SCIENCES

AND THE PRITZKER SCHOOL OF MEDICINE

IN CANDIDACY FOR THE DEGREE OF

DOCTOR OF PHILOSOPHY

DEPARTMENT OF BIOCHEMISTRY AND MOLECULAR BIOLOGY

BY

ALEXANDER R. FRENCH

CHICAGO, ILLINOIS

DECEMBER 2016

To my parents,

Robert A. French and Catherine E. French,

for teaching me to always

do my best

TABLE OF CONTENTS

List of figures vi

List of tables vii

List of abbreviations viii

Acknowledgments ix

Chapter 1: Prior work on optogenetics and myosins 1

1.1 Introduction 1

1.2 The *Avena sativa* LOV2 domain as an optogenetic engineering platform 2

1.2.1 Overview of optogenetic systems 2

1.2.2 Introduction to the PAS domain 3

1.2.3 The light-dependent conformational change of *Avena sativa* LOV2 8

1.2.4 Designing optogenetic tools with AsLOV2 11

1.3 Myosin VI: A motor protein that is activated upon binding cargo 15

1.3.1 The myosin head domain and its powerstroke 15

1.3.2 The myosin tail domain and themes of regulation in myosin motors 18

1.3.3 Unique features of myosin VI and its roles in the cell 23

1.3.4 The structure of the myosin VI cargo binding domain and its suitability for optogenetic control 26

Chapter 2: Recruitment and activation of myosin VI *in vivo* 29

2.1 LOVDab design and implementation in mitochondrial recruitment assay 29

2.2 LOVDab is a robust recruiter of myosin VI 33

2.3 Myosin VI recruits and activates myosin VI on peroxisomes 34

2.3.1 Myosin VI is recruited to peroxisomes via Dab2^{pep} 34

2.3.2 Myosin VI stalls peroxisome movement 36

2.4 Discussion of results and implications 39

2.5 Materials and Methods 40

Chapter 3: Purification and activation of myosin VI in *in vitro* gliding filament assay 44

3.1 Titer assay optimization 44

3.2 TIRF gliding filament assay shows LOVDab is capable of activating myosin VI 45

3.2.1 Demonstration of light-dependent activation with low [KCl] myosin VI 45

3.2.2 Re-optimization of myosin VI purification 47

3.2.3 LOVDab$_{+ctrl}$ activates myosin VI prepared in high salt 48

3.3 Evidence that myosin VI integrates cargo signals 52

3.3.1 Sensitization of myosin VI to protein cargo using PI(4,5)P_2 52

3.3.2 Myosin VI recruitment to the Golgi is uncorrelated with the amount of LOVDab on the membrane 52

3.4 Discussion of results and implications 54

3.5 Material & Methods 58

Chapter 4: Future directions and concluding remarks 61

4.1 Extending this work to studying myosin VI 61

4.2 Methods for improving the performance of LOVDab 64

4.3 Concluding remarks 67

Appendix A1: The LOV2 β bulge 68

Appendix A2: LOLOVV: a LOV2 within a LOV2 domain 69

Appendix A3: Light-dependent actin binding 73

References cited 77

List of figures

No.	*Title*	*Page*
1	The PAS fold	4
2	The LOV2 domain and its light-induced conformational change	9
3	Myosin classes and the mechanism of the myosin motor head	16
4	Structural and regulatory features of myosin VI	24
5	The myosin VI CBD and Dab2^{pep} co-crystal structure	27
6	Diagram of desired function of LOVDab	30
7	LOVDab robustly recruits myosin VI to different membranes within the cell	35
8	Myosin VI is recruited to peroxisomes via Dab2^{pep}	37
9	LOVDab reversibly recruits EGFP-myosin VI to peroxisomes in a light-dependent manner, which causes them to stall	38
10	In vitro gliding filament assay indicates that LOVDab activates full-length human myosin VI in response to light	46
11	Myosin VI purified in high salt binds actin reversibly and is recruited by LOVDab	49
12	EGFP-LOV2 fused to the myosin VI-binding portion of Optineurin migrates as a dimer by size exclusion chromatography	51
13	Lipid cargo sensitizes myosin VI to protein cargo Dab2^{pep}	53
14	Myosin VI integrates cargo signals when recruited to the Golgi	55
15	Model of myosin VI cargo integration in the cell	56
A2	LOLOVV maintains photocycle in both its constituent LOV2 domains	70
A3	MLLA actin binding assessed with the actin cosedimentation assay	74

List of tables

No.	*Title*	*Page*
A2	LOLOVV constructs and their linker sequences	72
A3	MLLA construct sequences	76

List of abbreviations

AA	Amino Acid
CD	Circular Dichroism
LOV2	Light, Oxygen, Voltage domain 2
EGFP	Enhanced Green Fluorescent Protein
Dab2	Disabled 2
$Dab2^{pep}$	A peptide fragment containing part or all of residues 674-711 from Disabled 2
UV-Vis	Ultra Violet to Visible wavelengths of light (in absorption spectroscopy)
FMN	Flavin Mononucleotide
TIRF/TIRFM	Total Internal Reflection Fluorescence Microscopy
DNA	Deoxyribose Nucleic Acid
PAS	Per-ARNT-Sim, Period-Aryl hydrocarbon Receptor Nuclear Transporter-Single-Minded
PYP	Photoactive Yellow Protein
PDZ	Post synaptic density protein 95, Drosophila disc large tumor suppressor, Zonula occludens-1 protein
NMR	Nuclear Magnetic Resonance
SDS-PAGE	Sodium dodecyl sulfate polyacrylamide gel electrophoresis

Acknowledgements

I would like to thank Tobin R. Sosnick and Ronald S. Rock for their mentorship throughout my time on this project. They both allowed me the freedom and great privilege of pursuing my own scientific ideas, which included finding many ways to not light-activate myosin VI, among them ideas that extended beyond the scope of my project. This required great patience and trust on their part, and I believe this contributed significantly to my growth as a scientist. I would also like to thank Kathleen Cheng and James Hastie, undergraduate researchers whom I mentored, for the work they did for me and their patience with me as well. Lisa Anderson and the BMB administrators deserve my thanks for all of the work they do behind the scenes to make sure this program runs smoothly. Likewise, I would like to thank all of the custodial staff and building engineers in GCIS and CSLC for keeping these buildings clean and in good operation throughout my time here. We benefit so much from their labor and I am not content to let their jobs be thankless ones. I also thank the Glotzer and Gardel labs for the use of their microscopes.

I would also like to thank my family for all of their love and support throughout the years, especially my parents, to whom I dedicate this dissertation. I also thank my wife, Elizabeth French, for all of her support and for making every moment more worthwhile. I give all glory to Christ for my work, and thank my church community for all of the encouragement and kindness they have shown to me. Lastly, I would like to thank my many friends here at the University of Chicago for all of the fun we have had throughout our time here and for helpful discussions on my research. I would like to thank my labmates in both the Sosnick and Rock labs for the same, and for making my place of work a productive and enjoyable one.

Chapter 1

Prior work on optogenetics and myosins

1.1 Introduction

Motor proteins play countless roles in biology, each requiring the motor to be recruited and activated at a particular time and place inside the cell. To dissect these multiple roles, we must develop tools that allow us to control the recruitment and activation process. One promising technique for achieving this goal is through optogenetics (4). Optogenetics involves the engineering and application of optically-controlled, genetically encoded proteins, and is transforming the fields of neuro- and cell biology (5, 6). A major benefit of optogenetics is that proteins are activated using light, which allows for high temporal and spatial control over their protein of interest.

Myosin VI is a motor protein whose study could particularly benefit from optogenetic control. It is the only myosin known to walk toward the pointed end of actin filaments (7, 8). This property enables it to perform a diverse array of cellular functions including cell division, endosome trafficking, autophagy, and Golgi and plasma membrane anchoring (9-12). Applying optogenetics to controlling myosin VI with light may therefore aid in the dissection of myosin VI's roles in different parts of the cell.

In this chapter, I first discuss the tools that are available to optogenetic engineering, with an emphasis on the *Avena sativa* LOV2 domain. I then review what is known about myosin regulatory mechanisms before discussing prior art on myosin VI regulation. Lastly, I outline the factors that make myosin VI amenable to control through the LOV2 domain.

1.2 The *Avena sativa* LOV2 domain as an optogenetic engineering platform

1.2.1 Overview of optogenetic systems.

One highly successful optogenetic strategy is to use or modify naturally-occurring light sensitive proteins that directly alter a cellular property of interest, such as using channelrhodopsin to manipulate membrane ion gradients (4). Another method is to fuse a target protein to a naturally light-sensitive protein that undergoes a conformational change in response to light. The new fusion protein is designed to sterically block the target protein's binding to its partner in the dark, but release it for binding in the light.

This latter engineering strategy has been employed using a variety of light-sensitive proteins, including cryptochromes (16), phytochromes (17, 18), photoactive yellow protein (PYP) (19), and the Light, Oxygen, Voltage sensing domain 2, or LOV2, from *Avena sativa* phototropin1 (20-22). Each system has its own benefits (4), which are discussed below.

Cryptochromes contain a photolyase-homology domain (PHD) that binds to both a flavin adenine dinucleotide (FAD) molecule that absorbs blue light and an additional flavin- or folate-derived cofactor that acts as an antenna system to shuttle near-UV light to the FAD (23, 24). In *Arabidopsis thaliana*, this chromophore is 5,10- methenyltetrahydrofolate (MHTF) (25). Upon absorption of light, the energy of the photon is converted to semi-reduce the FAD molecule to a neutral semiquinone radical (FADH·) (23). ATP binds in a pocket near the FAD chromophore and decreases the pKa of the nearby D398 residue (26). Upon light absorption, D398 donates its proton to FAD, creating a negative charge in this pocket that is thought to disrupt an interaction with the C-terminal region of the protein that exposes new interaction surfaces on the protein (25, 27). One consequence of this conformational change is that Cry2 proteins will self-associate into clusters (16, 28). The conformational change also allows them to bind to downstream

effectors, such as CIB1 in *Arabidopsis thaliana* (29, 30). Both of these effects have been used by optogenetic engineers to create time- and area-specific activation of protein activity (16, 29). Notable applications of these techniques include the regulation of endogenous receptors at the plasma membrane (31), as well as controlling the Cre DNA recombinase, a widely-used agent for tissue-specific manipulation of gene expression in higher organisms (32), with light in HEK293T cells (29).

While the clustering effect can give a large dynamic range to a switch, in some instances, including myosin studies, the oligomeric state of a protein may be essential to interpreting its activation state. Clustering complicates this interpretation. Cry2-based tools also exhibit dark state reversion on the minute to tens of minutes scale, making these unsuitable in cases where fast reversion is required (4, 16, 29).

Phytochromes, PYP, and LOV2 domains each take advantage of a modular signaling domain known as the PAS (Per-ARNT-Sim) domain, making this protein fold the most widely used optogenetic tool for applications outside of manipulating ion gradients through channelrhodopsins (4). Therefore, a more detailed discussion of this domain is warranted.

1.2.2 Introduction to the PAS domain

PAS (Per-ARNT-Sim) domains form a broad family of protein signaling domains that serve as detection modules for a diverse array of stimuli, and are found in every kingdom of life (33). The versatility of the domain is derived from its structure, which is an α-β protein fold composed of only 100-120 residues (34). The core element of the PAS domain is an antiparallel β sheet that contains five strands arranged in a 2-1-5-4-3 topological order (**Figure 1A,B**). Moglich et al. calculated the rmsd for the backbone atoms each pair of proteins among 47 PAS structures and

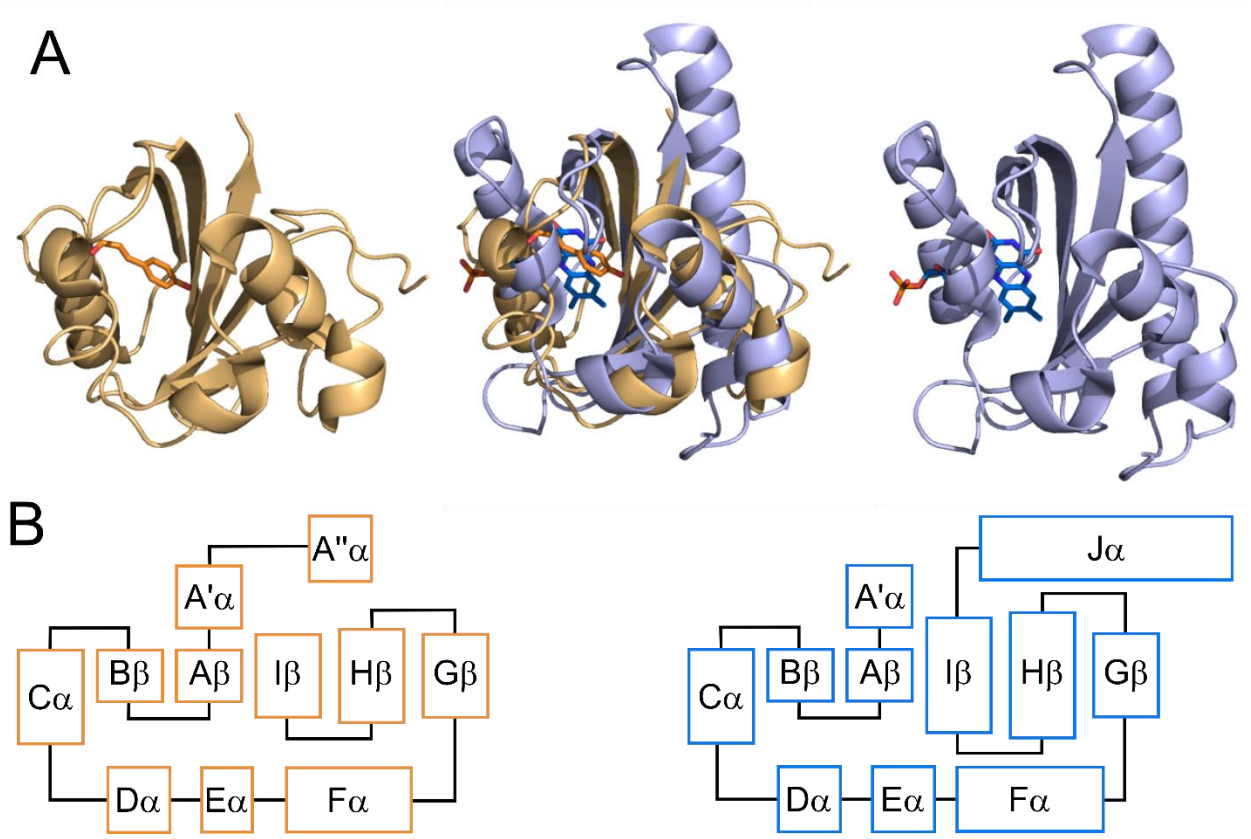

Figure 1. The PAS fold. (**A**) The *Halorhodospira halophila* PYP domain (bacteria) is shown on the left, and the *Avena sativa* LOV2 domain (plants) is shown on the right. *Center*: Overlaying the central β-sheet contrasts the relatively high conservation of the central PAS fold with the variability in the flanking helices. The different chromophores bind the conserved pocket on the front side of the β-sheet, with the output occurring on the opposite side of the sheet. Note that the conservation of the PAS fold spans kingdoms. (**B**) The domain architecture is laid out, with the length of the rectangles being roughly proportional to the number of residues in each structure. The 2-1-5-4-3 arrangement of the β-strands is clear.

found the average rmsd of these strands to be just 1.9 ± 0.6 Å (33). On either terminus and interspersed throughout the strands of the β sheet are helices. Typically, the primary sequence order of a PAS domain is Aβ-Bβ-Cα-Dα-Eα-Fα-Gβ-Hβ-Iβ. However, the length, orientation with respect to the β sheet, and even presence of these helices are not as well conserved as the central β sheet. Therefore, the β sheet is the central scaffold that defines the core of the PAS fold, whereas the helices vary from protein to protein, depending on its specific role (33).

This pattern of conservation suggests a biochemical mechanism by which each PAS domain senses its particular stimulus and propagates that signal to other protein domains, or effectors, which are often fused to the C-terminus of the PAS domain. In each case, the β sheet undergoes a conformational change in response to a physical or chemical stimulus that is then propagated to the effector through a linker domain on one side of the β sheet. This linker is often α helical and either forms coiled-coils or lies directly against the β sheet, as is the case for the C-terminal Jα helix of the *Avena sativa* LOV2 (Light, Oxygen, Voltage) domain (35).

On the opposite side of the sheet, many PAS domains bind cofactors that can either aid in the detection of a stimulus, such as the absorption of blue light by a bound flavin mononucleotide (FMN) in the LOV2 domain (36), or can serve as the signal itself, as in the citrate sensor CitA, which undergoes a conformational change in response to binding citrate (37). The PAS β sheet curls in towards one of its faces, forming a conserved pocket in which the cofactor binds. Capping the pocket are the Eα and Fα helices, which are customized to fit each cofactor. Though many PAS domains do not require a cofactor, the pattern of conservation and cofactor binding in those PAS domains that do bind small molecules suggest a general signal transduction mechanism whereby signal-specific helices on one side of a conserved β sheet cause a conformational change in the sheet that is propagated to effector-adapted helices on the opposite

face of the sheet. This propagation can occur through a variety of mechanisms that each depend on thermodynamically coupling the effector domain of interest to the conformational change in the PAS domain, such as through alteration of the oligomeric state of the protein (38), relief of steric inhibition (39, 40), or direct stabilization of the effector (41).

The ability of PAS domains to control the function of diverse effector proteins lends them to applications in protein engineering, including optogenetics. The Moffat group has previously engineered a light-dependent response into a PAS:effector protein pair that already has the desired output (42). They did so by testing a series of constructs where the PAS-gated histidine kinase FixL from *Bradyrhizobium japonicum* had its N-terminal PAS domain substituted with the light-sensitive LOV domain from the *Bacillus subtilis* YtvA protein. Excitation of their optimal construct, "YF1", causes FixL to phosphorylate its transcription factor target FixJ. YF1 shows a 60-fold change in response to light in an *in vivo* β-galactosidase assay where the LacZ gene was put under the control of the FixJ promoter of FixJ (42).

While engineering a light-dependent response into a PAS:effector protein pair that already has the desired output is possible, more often the preferred approach is to reengineer a light-responsive PAS to control a non-native effector (33, 42). There are several protein families within the PAS superfamily that react to light. Phytochromes are dimers of two, 125 kDa proteins that covalently bind to a tetrapyrrole chromophore within a GAF (cGMP phosphodiesterase/adenyl cyclase/FhlA) domain that is highly integrated with a PAS domain (43). In the case of *Arabidopsis thaliana* PhyB, which has been used to control proteins optogenetically (17, 18), the chromophore is a molecule of phycocyanobilin (PCB) that isomerizes upon illumination with red ($\lambda_{max} \approx 655$ nm) light (44, 45). This isomerization causes a conformational change in the "tongue" region of the phytochrome domain (PHY) that then

causes each PHY domain to move away from each other and more closely to their respective intrachain PAS-GAF domains (46). In the case of PhyB, this structural rearrangement enables it to bind the transcription factor phytochrome interaction factor 3 (PIF3) (47). Pfr, the red-light excited, biologically active form of PhyB, can be reverted to its inactive form Pr using far-red ($\lambda_{max} \approx 735$ nm) light (45). By tethering target molecules to PhyB and PIF3 in mammalian cells, Levskaya *et al.* were able to create an optogenetic protein recruitment system (18). By projecting patterns of 650 and 750 nm that were inverse to each other they demonstrated precise patterning of light-induced recruitment to the plasma membrane, with almost no activity outside the area excited with the 650 nm laser. By fusing the PIF to a RacGEF that promotes lamellipodia formation in cells, they could use this system to induce lammelipodia protrusion at precise places in the cell (18).

The PhyB system is advantageous since the bidirectional reversion allows for precise control of protein activation. However, in most organisms the chromophore must be added to the system exogenously, or additional genetic work must be done to give the organism the ability to synthesize the chromophore themselves (18). Additionally, the large size of the proteins may make it unsuitable for some applications.

Other light-reactive PAS families include the photoactive yellow protein (PYP) and LOV domain. PYP binds a *p*-coumaric acid molecule that absorbs light with $\lambda_{max} \approx 446$ nm (48, 49). PYP domains are found in bacteria where they regulate negative phototaxis (50). Similarly, LOV domains absorb light with $\lambda_{max} \approx 447$ nm (36) through binding to either an FMN or FAD cofactor (33). These domains are found in plant phototropins where they upregulate a variety of large scale plant responses to light, including phototropism (51). Though PYP has been successfully applied to controlling the DNA binding of several proteins, including the

transcription factor CREB, with light (19, 52, 53), LOV domains have been used more frequently in optogenetic applications (54). This is possibly due to the fact that FMN/FAD cofactors are available in all living systems, whereas *p*-coumaric acid must be added exogenously to PYP outside of its native organism (52). Among LOV domains, the *Avena sativa* LOV2 domain has proven to be a robust optogenetic tool capable of being engineered to control a variety of proteins, due in part to its small size and relatively straightforward mechanism for caging a peptide (21, 22, 41, 55). This protein is discussed in detail in the following section.

1.2.3 The light-dependent conformational change of *Avena sativa* LOV2

The ~150 AA *Avena sativa* LOV2 domain binds a flavin mononucleotide (FMN) cofactor with $\lambda_{max} \approx 447$ nm and undergoes a conformational change involving the unfolding of its N-terminal A'α helix and the much larger, C-terminal Jα helix upon absorbing blue light (**Figure 2A**) (36, 56, 57). Specifically, upon absorption the FMN passes through an excited triplet state before being quenched by the formation of a covalent bond between the FMN's C4a atom and the sulfur atom of the catalytic cysteine residue C450 (58, 59). This reaction has a quantum yield of approximately 0.5 and requires the donation of a hydrogen atom to the N5 atom of the FMN ring (60), which then alters the electrostatic environment around a conserved amino acid in the FMN binding pocket, Q513 on the Iβ strand (**Figure 2B**) (61, 62). It was originally speculated that Q513 moved from hydrogen bonding the O4 to the newly protonated N5 atom and that this shift caused a change in the β sheet that disfavored Jα helix docking (62). This mechanism is supported by recent time-resolved vibrational spectroscopy experiments suggesting that Jα helix unfolding begins concomitantly with changes in β-sheet structure in LOV2 (63). However, MD

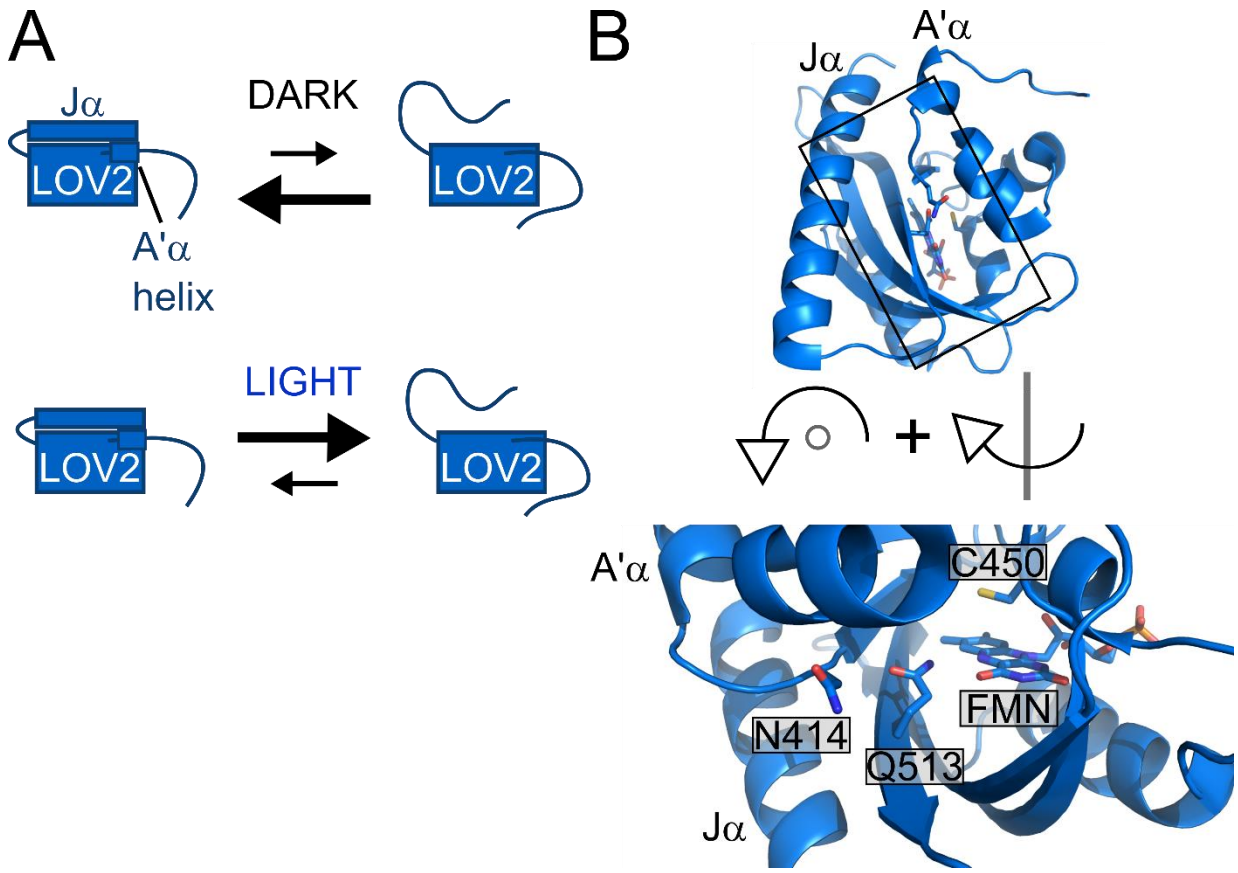

Figure 2. The LOV2 domain and its light-induced conformational change. (**A**) Cartoon illustrating the conformational change in the LOV2 domain. The terminal helices go from primarily occupying a rigid, folded state in the dark to a flexible unfolded state in the light. (**B**) *Top*: a view of the LOV2 domain showing its output helices, the A'α helix at its N-terminus and the Jα helix at its C-terminus, that unfold upon absorption of light. *Bottom*: rotated view of LOV2 core shows interacting residues N414 and Q513. The catalytic cysteine residue C450 is represented in sticks as well. Coordinated motions of Q513 and N414 are thought to drive the unfolding of the A'α and Jα helices.

simulations (64) and mutational studies (57, 65) suggest that upon C450 adduct formation Q513 maintains a variety of hydrogen binding partners, including a water molecule that bridges the Q513-N5 bond in the lit state of LOV2. It also swings away from the FMN altogether, interacting with N414, which is adjacent to the Aβ strand (64). N414 is thought to play a role in setting the solvent accessibility of the FMN. Accordingly, the photocycle lifetime is highly sensitive to mutations at N414 (57, 65).

Additionally, since N414 is immediately adjacent to the Aβ strand, which lies under the A'α helix, the coupled motions of Q513 and N414 are thought to destabilize the A'α helix (**Figure 2B**). This, together with the twisting of the Iβ strand through changes in the FMN binding pocket, are hypothesized to be the primary drivers of the light-dependent unfolding of the Jα helix (57, 63, 64). Despite the above evidence for Q513 driving these structural changes, mutation of either Q513 or N414 does not completely abolish the photocycle (57, 65). Thus, though the motion of Q513 may be the primary upstream driver of the unfolding of the A'α and Jα helices, the exact mechanism of signal transduction in LOV2 and its parent protein phototropin1 is still debated (66).

When the light stimulus is removed, the C450-FMN bond spontaneously hydrolyzes in the dark on the seconds to minute time scale followed by rapid refolding of the A'α and Jα helices, thus completing the photocycle (56, 57, 59). The degree of this conformational change and the rate at which the helices refold in the dark can be independently altered by mutation (57, 67) which can be useful for tuning a photoswitch (20, 21). I discuss this practice and the general methodology used to design a photoswitch in the following section.

1.2.4 Designing optogenetic tools with AsLOV2

Previously, the Sosnick and Moffat labs engineered the LOV2 domain to control DNA binding by fusing the tryptophan repressor (TrpR) to the C-terminus of the LOV to create a LOV2-and-Tryptophan-Activated-Protein, or "LovTAP" (41). They did so by fusing the Jα helix to the N-terminal helix in TrpR in such a way that the folding of the Jα helix sterically prevents TrpR from occupying its dimerized, DNA-bound conformation. The activity of TrpR was thus coupled to the light-dependent conformational state of the Jα helix, creating a protein showing light-dependent DNA binding (41).

Similarly, their next design, a collaboration with the Glotzer lab, sterically blocks, or "cages" a small PDZ domain-binding peptide that was fused to the C-terminal Jα helix (21). In this system, called Tunable Light-controlled Interacting Proteins, or "TuLIPs," the light-induced unfolding of the Jα helix uncages a peptide that then binds a PDZ domain. Since light triggers the association of the LOV-peptide and PDZ domain, the association of any two proteins *in vivo* can be made light-dependent by fusing one partner to the PDZ domain and the other to the LOV2-peptide. This strategy has been utilized by several groups for the control of a variety of protein-protein interactions (54) including most recently epigenetic modifications (68).

Whether the objective is to control a peptide (21), a small protein such as a transcription factor (41), or a kinase (22), the general strategy involved is to couple the conformational states of the LOV2 domain in the light and dark with the active and inactive states of the target protein, respectively (20). The conformational change in LOV2 is best thought of as a shift in the equilibrium constant of the Jα helix for the LOV2 domain from a tight binding state in the dark to a weakly binding state in the light (**Figure 2A**) (69). Following this line of thought, Yao *et al*. used NMR spectroscopy to estimate the amount of free energy available for coupling in the

LOV2 conformational switch by calculating the free energy change resulting from the shift in percent occupancy of the folded state of the Jα in the light and dark (69). They found it to be approximately 4 kcal/mol (69). This is far less than the 60-70 kcal/mol of energy expected from a typical blue photon absorbed by the LOV2 FMN. Various factors, including the sampling of multiple energetically favorable orientations by Q513 in the lit state likely contribute additional "slippage" to the switch (64). Nonetheless, 4 kcal/mol, equivalent to a fold change of about 600x in the Jα helix docking equilibrium constant, is far above the dynamic range of LOV2-based optogenetic tools made to date (54). Viewed from a positive angle, this means that the LOV2 domain contains plenty of energy for the formation of effective switches. However, it also shows that there is much more left for engineers to learn in order to take advantage of the full range of power of the LOV2 domain conformational change.

To further illustrate the considerations taken into account when engineering an optogenetic tool, we can look at the example of engineering light-controlled binding of an "activator" peptide to an "effector" protein. Most often, as in natural proteins, the most effective method is to fuse the peptide to the large Jα helix on the C-terminus of LOV2 to form a LOV2-activator fusion protein (33). As discussed above, the maximum free energy available in the Jα helix conformational change translates into a maximal change in activity for LOV2-based tools of approximately 600-fold. Therefore, the challenge is to tune the light- and dark-state affinities of the LOV2-activator for the effector to a level where a meaningful difference in complex formation will be observed. This level necessarily depends on the concentration range that one expects the proteins to exist at in the cell. Viewing this from the extremes, at a high effector:LOV-activator ratio, if the concentrations of both partners are well below the K_D of the interaction then even a 600-fold increase in the availability of the peptide may not yield an

observable amount of bound effector. At the other end, it is clear that if the protein concentrations are above the dark state K_D, then the effector will be captured even in the dark state and no change will be observed, even for a 600-fold elevation in peptide availability in the light. Therefore, the observability of light-dependent activation is dependent on the concentration of the proteins being studied. In addition to guiding the engineering process, this concentration dependence also makes it important that the optogenetic experimentalist optimizes his or her expression protocol to obtain consistent expression levels of each protein of interest in their cellular system.

Maximizing the dynamic range of the switch also requires the LOV2-activator to be designed so that the binding site of the activator for the effector is sterically blocked by the LOV2 domain when the Jα helix is folded in the dark state. In the above example, this design process involves truncating residues from the Jα helix-activator fusion site to bring the binding site of the effector as close to the LOV2 domain as possible. This truncation also shifts the helical register of the binding site, so that in effect only sequences where the key binding residues of the activator are facing in toward the LOV2 domain need to be considered. However, as one begins to alter the sequence of the Jα helix, the affinity of the helix for the LOV2 domain may be altered, and is typically destabilized (20). In particular, disruption of the interaction between I539 on the Jα helix and the LOV2 core partially unfolds the Jα helix (70). Therefore, mutating residues N-terminal to I539 is to be avoided, unless the activator has significant homology to the Jα helix (40), or when beneficial mutations are found *a posteriori* during mutagenesis screens (55). Once the LOV2-activator has been designed to eliminate binding to the effector in the dark state, compensatory mutations in the LOV2 domain are made to re-stabilize the folded state of the Jα helix. The degree of light-dependent conformational change in many LOV2 mutants has been

characterized by circular dichroism (CD) and nuclear magnetic resonance (NMR), with their corresponding photorecovery kinetics interrogated via UV-Vis spectroscopy (57, 67). Using different mutations, these two properties can be altered independently to tune the strength of the Jα helix docking affinity and the photocycle kinetics to the desired level for the system of interest.

One particularly useful double mutation that was found in a rational search of LOV2 mutants is the T406A/T407A mutation on the A'α helix. As discussed above, the A'α helix plays a role in stabilizing the folded state of the adjacent Jα helix (57). Therefore, stabilizing the A'α helix may stabilize the Jα helix through their interaction in a linked equilibrium. The T406A/T407A is thought to accomplish this by replacing threonine residues with alanine, which has a higher helical propensity than Cβ-branched amino acids. The increased helical propensity of the A'α helix stabilizes its folded state, which then contributes to the Jα helix stability. CD data shows that LOV2 domains with this double mutation have a larger fractional change in helicity between lit and dark states than the wild type protein (57). In combination with its use in several optogenetic tools to suppress dark state binding of LOV2-activator fusion proteins (21, 71), these data suggest that this mutation works to stabilize the Jα helix in the dark.

Other mutations have also been successfully used in optogenetic design. For example, G528A and I532A mutations on the Jα helix are thought to stabilize it by directly increasing its helical propensity (20, 21, 71). In practice, a battery of mutants are selected for testing when designing an optogenetic switch. This is made possible by the robustness of the photocycle in the LOV2 domain, which allows it to serve as a uniquely tunable platform for optogenetic engineering.

1.3 Myosin VI: A motor protein that is activated upon binding cargo

1.3.1 The myosin head domain and its powerstroke

There are three superfamilies of motor proteins: kinesins, dyneins, and myosins. Kinesins and dyneins walk on the micotubular component of the cytoskeleton, whereas myosins walk on actin (72). Kinesins move toward the + end of microtubules, generally toward the cell periphery, whereas dyneins move exclusively toward the – ends of microtubules, or generally towards the cell center. Therefore, each of these superfamilies of motor proteins play a distinct set of roles in the cell. As discussed in **Section 1.3.3** below, a particular class of myosin, myosin VI, is particularly amenable to control by optogenetics. I therefore focus on reviewing myosins. I will also point out similarities between myosins and the other motors where convenient in order to understand the generalizability of optogenetic control of myosins to understanding motor proteins.

There are at least 35 families or classes of myosins known to date, with at least 12 expressed in humans (73, 74). The number of classes of myosins is expected to grow as more species' genomes are sequenced (75). Classes that are so-called "conventional" myosins form filaments and are involved in force-generation and contraction processes such as cytokinesis or muscle movement (**Figure 3A**) (72). The remaining "unconventional" myosins are recruited to various cargoes in the cell where they act as either dimers or monomers to maintain force on the actin cytoskeleton in either transport or tethering roles (72).

Myosins each share a highly homologous, approximately 80 kDa actin-binding ATPase domain on their N-terminus and vary widely in their C-terminal domains (75, 76). Generally speaking, the nucleotide state of the ATPase determines the affinity of the myosin for actin (**Figure 3B**). When the nucleotide pocket binds either ATP or ADP-Pi, the head domain has only

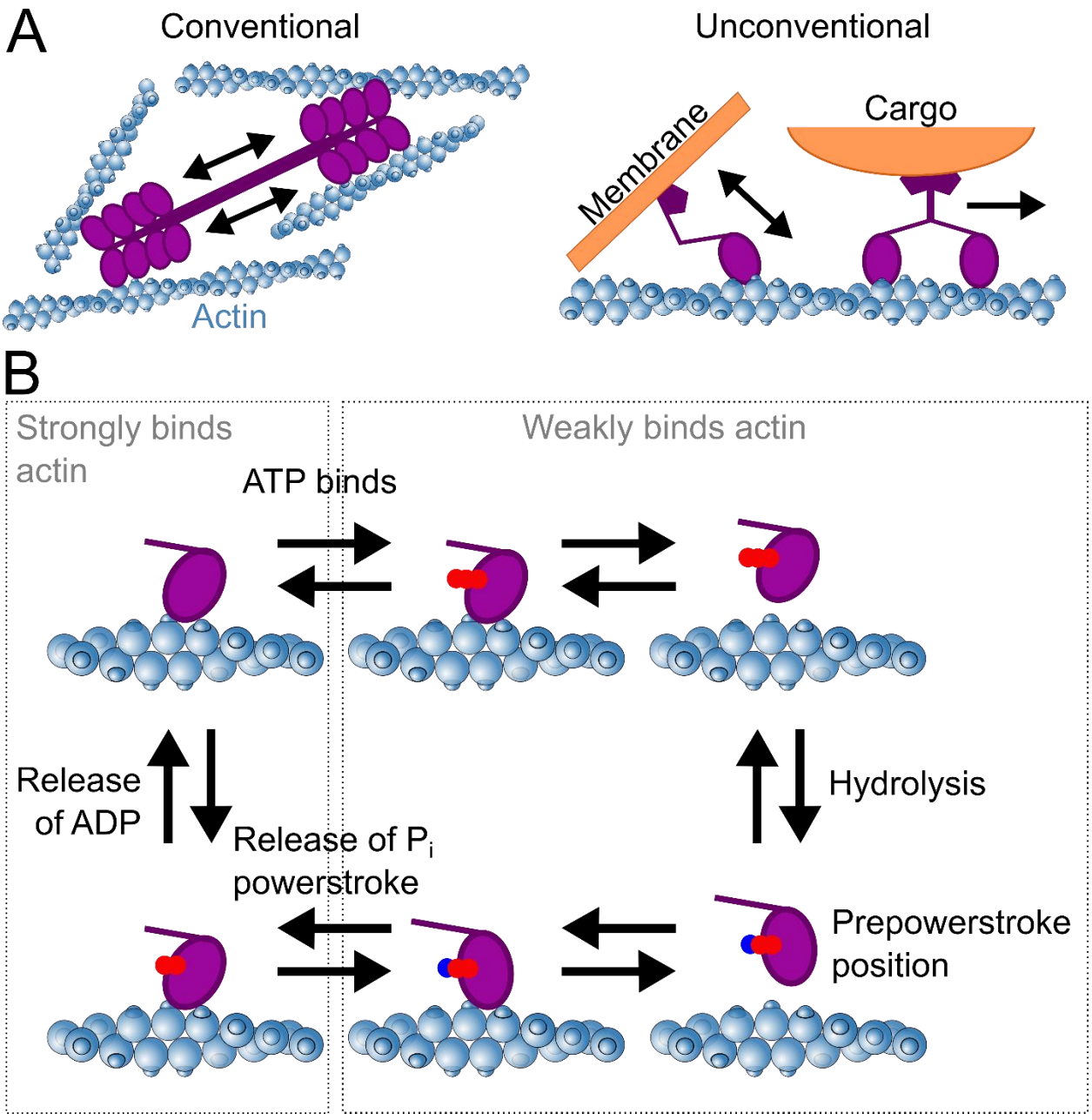

Figure 3. Myosin classes and the mechanism of the myosin motor head. (**A**) Conventional myosins form filaments through their C-terminal tail domains in order to generate force between actin filaments. Unconventional myosins have cargo binding domains that allow them to sense or generate force between the actin cytoskeleton and cargo, often a membrane-bound organelle in the cell. These can operate as monomers or dimers. (**B**) ATP cycle of myosin head. When myosin binds ATP, the affinity for actin is decreased. Hydrolysis to the myosin:ADP:P_i state puts the myosin head in the prepowerstroke state (note the tilt of the oval motor domain). Binding to actin accelerates the release of P_i (blue dot) causing the myosin head to move through its powerstroke. The myosin in the ADP and apo states has a high affinity for actin, staying bound until ATP binds and the cycle resumes.

weak actin binding. Hydrolysis of ATP to ADP-P_i causes the head domain to undergo a conformational change involving a large swing of its converter and/or lever arm domains that lie just C-terminal to the head group. This puts the myosin in a "prepowerstroke" condition. Myosin then binds to the actin, accelerating the release of the phosphate group (77). P_i release causes the conformational change that set the prepowerstroke position of the lever arm to reverse (78). This swing is referred to as the "powerstroke" of the myosin, and is the force-generating portion of the ATP cycle. When in the ADP-bound or apo states, the myosin head binds tightly to actin. Since myosin bound to either ATP or ADP-P_i binds only weakly to actin, ATP binding to apo myosin effectively releases the myosin head from the actin filament. Thus, the cycle is completed and the myosin is free to take a new powerstroke or step along the actin (79).

Though kinesins, dyneins, and myosins differ, each motor protein superfamily shares the common mechanism of coupling an ATP hydrolysis states to altering the affinity of a track binding domain. For kinesins, ATP hydrolysis and subsequent P_i release promotes the unfolding of the N-terminal 2.5 turns of the H4 helix, which binds in the interface between α- and β-tubulin monomers (80, 81). For dyneins, a AAA+ domain causes a shift in its coiled-coil stalk domain upon ATP binding. This shift causes a conformational change in the dynein microtubule binding domain (MBD), exposing the H1 helix in the MBD which binds tightly to microtubules (82). The changes in affinities for the microtubule track are likewise coupled to conformational changes in kinesins and dyneins that promote the binding of the detached monomer to binding in front of the attached monomer (81, 82). The exact mechanisms of how this is accomplished in these two superfamilies is still debated (83, 84).

The percentage of time that a myosin is bound to actin is referred to as its "duty ratio." A high duty ratio is necessary for those myosins that act as transporters to fulfill their cellular

functions. These myosins associate to form dimers. They are kinetically tuned so that the myosin heads alternate powerstrokes, allowing them to take multiple steps in a hand-over-hand fashion along the actin filament. A high duty ratio is necessary to ensure that the head that is unbound from actin has enough time to hydrolyze its new ATP molecule, rebind to actin, and release P_i. For this reason, ADP release is often the rate-limiting step for myosins. The position of the nucleotide binding pocket relative to the lever arm – and therefore the direction of the intramolecular tension arising from pulling cargo – is thought to ensure that pocket in the leading head undergoes compression, slowing the ADP release. This idea is supported by the different kinetics of myosin VI (85). Myosin VI is the only unconventional myosin that walks toward the pointed end of filaments (7). Myosin VI must therefore experience intra cargo-actin strain from the opposite direction than other myosins, meaning that ADP release could not be the rate limiting step (86). Despite this, myosin VI has a high duty ratio just as other transport myosins (77, 86). Myosin VI manages this high duty ratio through a small, 25 amino acid insert near its nucleotide binding pocket, called insert-1 (87, 88). Once ADP is released, this insert promotes a slight structural change in the lead head of the myosin VI dimer that prevents ATP from binding, thus prolonging the amount of time myosin VI is bound to the actin (88, 89).

1.3.2 The myosin tail domain and themes of regulation in myosin motors.

Though myosins show some variability in their N-terminal motor domains, their C-terminal tail domains show the most diversity (74, 90). The diversity in the tail domains of myosins is reflective of the diverse cellular roles carried out by this superfamily of proteins (75). The localization of this diversity to the tail domains is due in part because the tail domain is where the myosins bind to their cargo, and in the case of conventional myosins, where they oligomerize

into filaments. This structural arrangement is necessary since if the myosin heads bound to their cargo they could not move relative to their cargo during the powerstroke of the ATP cycle, preventing them from generating force.

The tail domains also play a large role in regulating myosin activity. Given their ability to create large scale changes in organelle shape and dynamics, myosin activity is tightly regulated in the cell. Regulation occurs on three levels: transcription of splice variants; intra- and intermolecular binding to regulatory molecules or protein domains, including cargo; and through the actin, which modulates the myosin head directly (75).

Humans have 38 genes for myosins that belong to twelve classes (73, 74, 91). Barring systems with intentional redundancy, this leaves room for much time- and site- specific selection of myosins at the transcriptional level. The myosin V class, for example, has three genes in humans that each have different regulatory mechanisms and cargo in the cell (75, 92). In fact, while myosin Va and Vb are processive dimers with high duty ratios and walk on actin filaments, myosin Vc has a low duty ratio and only moves processively on actin bundles as a single motor dimer (92, 93). The stark variety in these myosins underscores the importance of being able to transcriptionally control myosins in a cell and cargo-dependent manner. Myosin VI on the other hand, is regulated through alternative splicing (9). In humans, myosin VI has four splice isoforms that each contain a different combination of two inserts in its tail domain, referred to as the short insert (9 AA, SI) and the long insert (21-31 AA, LI) (9, 94). Different splice isoforms are differentially expressed in different tissues, and the effects of the presence or absence of either insert are tissue-specific (9, 94). In some polarized cells, the presence of the LI is necessary for binding to clathrin coated vesicles (9), whereas in some cell lines myosin VI may not target to clathrin coated pits at all, depending on the cargo proteins expressed in that cell

line (94). Though the exact impact of each splice form is clearly nuanced, the no insert and small insert splice forms are generally preferred for vesicle sorting and Golgi maintenance (13, 95, 96), whereas isoforms containing the large insert are generally required for interaction with clathrin coated vesicles (9, 94). This level of regulation in myosin VI is not essential for mammalian life, since porcine myosin VI lacks both inserts (94).

Once translated, myosin activity is further controlled through interactions with a variety of proteins and small molecules. Members of nearly every myosin class are phosphorylated, with the best studied example being the conventional myosin II (75). These myosins can have multiple phosphorylation sites in their tail domains, where phosphorylation usually promotes the disassembly of the myosin II filaments (75). In contrast, phosphorylation of associated proteins, or light chains, to the myosin II molecules usually upregulate activity of the motor, and in mammalian smooth muscle are the major control point for myosin II activity (97).

A phosphorylation site that is conserved in both conventional and unconventional myosins is the so-called TEDS (Threonine (T), Glutamic acid (E), Aspartic acid (D), Serine (S)) site (98). This site on the motor domain is conserved across motor classes as either a phosphorylatable T/S residue or a negatively charged phosphomimetic D/E residue (98). Myosin VI is at least partially regulated at this site, as phosphorylation of this motor targets it to membrane ruffles and may influence how it interacts with actin in the cell (99, 100). Myosin 1, a structurally similar motor to myosin VI, is also regulated through phosphorylation. Phosphorylation at the TEDS site may increase ATPase activity and actin affinity by more than 20 fold in these motors (75). Some myosins rely on phosphorylation so heavily they actually evolved to have kinase domains as part of their architecture. Mammalian myosin IIIs contain kinase domains N-terminal to the motor

domain that autophosphorylate before phosphorylating multiple sites on the motor head to inactivate the protein (75).

Myosins of classes II, V, VII, and X each show autoinhibition of the ATPase domain by their tail domains (75). Electron microscopy (EM) of class Va myosins shows that the tail domains in a myosin Va dimer fold up to interact with the motor domains to inhibit hydrolysis (101, 102). EM studies later revealed a similar mechanism for myosin VIIa (103, 104). Interestingly, though the enzymatic properties of the myosin VI ATPase do not appear to be altered by its tail domain, it seems that myosin VI is a folded up monomer in the absence of cargo (105-107). Details of this are discussed further in the following section.

Given that myosins are ATPases, it is no surprise that Mg^{2+}, a common cofactor in ATPases that coordinates the multi-charged phosphate tail of nucleotides in the ATPase active site, can affect myosin activity (75). Another important ion for myosin regulation is Ca^{2+}. This ion commonly binds to myosin light chains, such as calmodulin domains that bind to the neck region of unconventional myosins, as well as the essential light chain (ELC) in conventional myosins. The effect of Ca^{2+} is myosin-specific. For example, Ca^{2+} binding to myosin I causes its CaM to dissociate from the lever arm, resulting in flexibility in this domain. The result is a less efficient motor (108). In contrast, Ca^{2+} binding to the ELC:RLC complex on some myosin-IIs causes the neck region to rigidify, relieving the myosin autoinhibition and leading to their activation (75).

Conformational changes have also been observed upon addition of Ca^{2+} to class V and VI myosins, suggesting that Ca^{2+} transients, common in cells, can help regulate myosin activity (92, 109). In myosin V, Ca^{2+} can completely relieve the autoinhibition of the head domains and cause myosin V to become processive (92). Pulses of Ca^{2+} have similarly been shown to activate myosin VI in the presence of certain lipids (109). The physiological relevance of these

phenomena are still disputed, however. Ca^{2+} binding dissociates the CaM from the myosin V neck, reducing its stiffness and the overall efficiency of the motor, suggesting this would not be a reasonable activation mechanism (110). For myosin VI, multiple previous studies showing activation of the molecule in the absence of Ca^{2+} suggest it is not essential for its function (106). More work is required to fully understand the interaction of myosin VI and Ca^{2+}.

However, one clearly relevant Ca^{2+}-based myosin regulatory mechanism is through the actin track. In striated muscle, myosin II is completely regulated through conformational changes in actin-bound tropomyosin-troponin complexes (75). These actin-bound proteins change conformation to reveal the myosin binding site on actin upon binding Ca^{2+} that is released from the sarcoplasmic reticulum during muscle contraction (111). Numerous troponins are expressed that regulate the behavior of nonmuscle myosins as well (75).

Interestingly, the time and area-dependent conformation of the actin track can also influence myosin behavior. Actin is itself an ATPase, and the nucleotide state of a given monomer depends on how long it has been incorporated into a filament, with "fresh" filaments being composed of actin in the ADP-P_i state and older filaments having monomers primarily in the ADP state (112). The nucleotide state of the filament affects its flexibility through conformational changes one of its subdomains (113). Myosin V and myosin VI have opposite preferences for young and old filaments, with myosin VI having longer run lengths on old actin (114).

Myosins can also have preferences for certain actin structures. Myosin X for example, has been shown to only walk on actin bundle (115). This feature may help myosin X to diffuse faster to cellular structures containing these bundles such as filopodia, where it fulfills its biological function (115). The degree of this preference is still debated in the literature (75), and depends on the exact orientation of the dimerization domain of myosin X (116, 117).

Myosins are a diverse group of proteins that generate mechanical force in the cell by hydrolyzing ATP to cyclically interact with the actin cytoskeleton. The diversity in myosin regulatory mechanisms reflects both their diverse roles in the cell as well as their general importance to the cell. Within the myosin superfamily, only myosin VI walks toward the pointed end of filaments. This, together with the myriad of myosin VI regulatory features discussed above, makes this protein particularly interesting – and particularly challenging – to study. A more detailed discussion is warranted to understand the distinctive properties of this motor.

1.3.3 Unique features of myosin VI and its roles in the cell

Myosin VI is the only myosin to walk toward the pointed end of actin filaments (7, 8). It accomplishes this feat through two small inserts in its motor domain, referred to simply as "insert-1" and "insert-2" (**Figure 4**). As discussed in the previous section, insert-1 is positioned near the ATP-binding pocket of the motor head and prevents ATP binding to the lead head of the myosin VI dimer as a means of gating the lead head as it experiences strain (88). Insert-2 is comprised of 39 residues located just C-terminal to its converter domain. Replacement of insert-2 with the lever arm of a barbed end-directed motor is sufficient to make myosin VI walk toward the barbed end of filaments. Thus, while insert-1 is important for load-dependent ATP activity, insert-2 is sufficient to reverse the direction of myosin VI (118, 119). Insert-2 forms a helix that is bent to form many contacts with the converter domain, effectively swinging the lever arm 120 degrees relative to that of other myosins (88). These contacts are presumed to promote a large structural rearrangement of the converter domain that together cause a 140 degree swing in the lever arm through the powerstroke, twice the value seen for myosin II (120). The structures of the pre- and post-powerstroke states therefore predict a lever arm motion of 12 nm, in agreement with what was measured for S1 fragments of myosin VI (121).

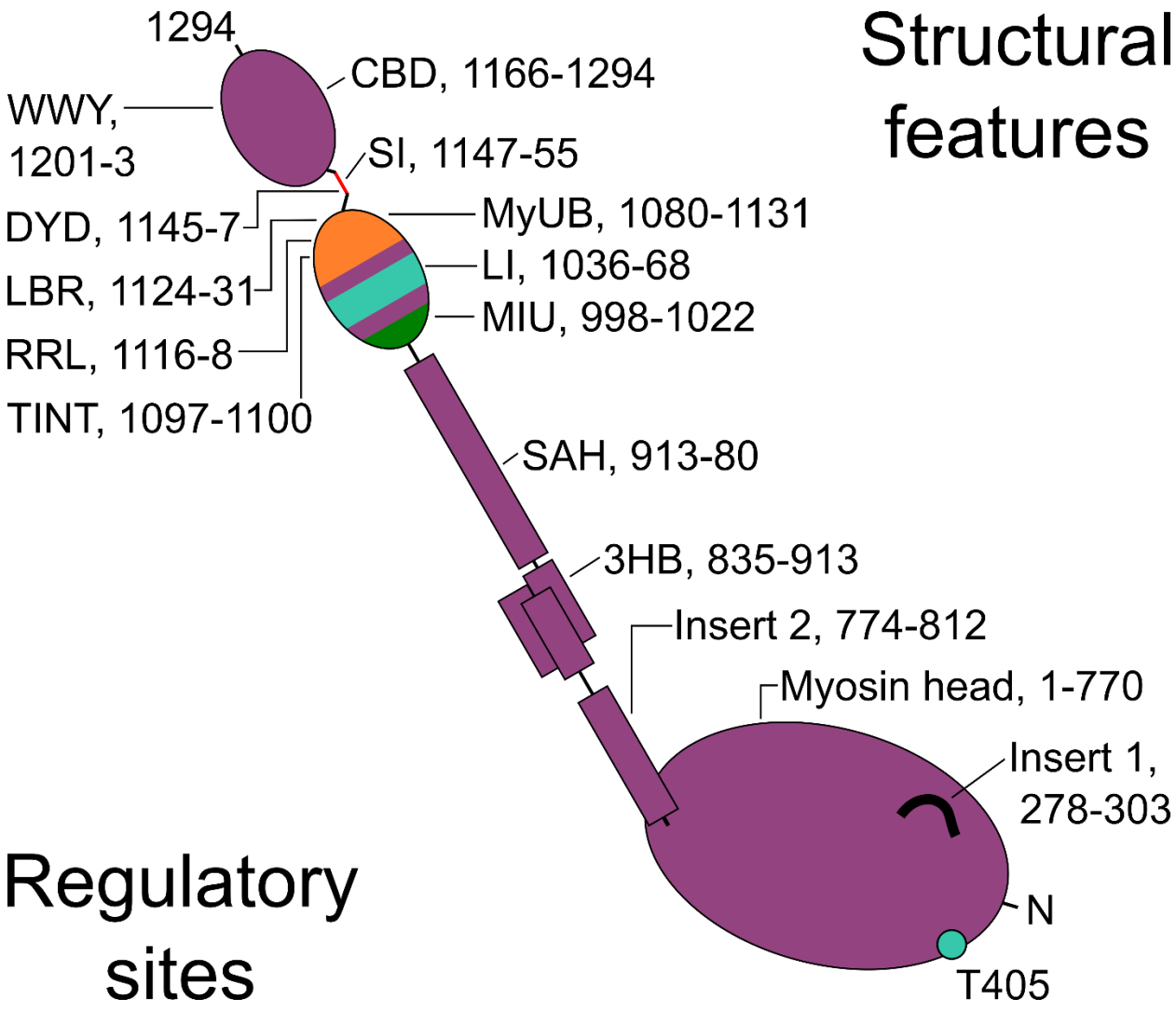

Figure 4. Structural and regulatory features of myosin VI. Numbers are residues based on human myosin VI (UNIPROT ID: Q9UM54). *Structural features*: 3HB: three helix bundle, SAH: single alpha helix domain, MIU: motif interacting with ubiquitin, LI: Large insert, MyUB: myosin ubiquitin binding domain, SI: small insert, CBD: cargo binding domain. *Regulatory sites*: T405, TINT, DYD are residue codes for phosphorylation sites on myosin VI. RRL and WWY are conserved residue triplets required for binding to optineurin- and Dab2 class cargoes, respectively. LBR: lipid binding region.

The full 36 nm step size of myosin VI allows it to span the half-helical twist in the actin filament and maintain its track on the same face of the filament. This type of stepping prevents the myosin from spiraling around the filament and generating torsional strain. The 3HB unfolds when myosin VI is activated and extends its lever arm, accounting for the full step size of myosin VI (105).

Given its unique position as the only pointed end-directed myosin, it is perhaps no surprise that myosin VI plays many important roles in the cell (122). These include transporting endocytic vesicles through cortical actin (94, 123, 124), regulating receptor-mediated trafficking (125), maintaining Golgi morphology (13), and coordinating the fusion of autophagic vesicles to lysosomes (12), among others (122). Functional myosin VI has also been shown to be critical for specialized structures in spermatid development (126, 127), and for the maintenance of microvilli in a human colonic cancer (Caco-2) cell line (128) and of stereocilia in inner ear hair cells (129-131). Furthermore, its roles in cell migration are thought to partially explain its upregulation in ovarian and prostate cancers (132-134).

Myosin VI is able to accomplish these diverse roles through its C-terminal cargo binding domains (CBDs), which bind to a vast array of adaptor proteins, called “cargo” proteins, that recruit myosin VI to its various membranes of action in the cell. (76, 122, 135). These cargo proteins can be grouped into two classes that bind to distinct, conserved motifs on the myosin VI C-terminus (76). Disabled2, or Dab2, belongs to the class of cargo proteins that bind to a conserved WWY site on myosin (**Figure 4**) (136). Optineurin (OPTN) is a member of the other class, whose members bind to a conserved RRL motif (13).

In addition to controlling where in the cell myosin VI is recruited, these cargo proteins also determine where myosin VI is active. The distinction between active and recruited is necessary

since, as discussed above, myosin VI is one of several myosin classes that are auto-inhibited (75). When myosin VI binds to its cargo, this auto-inhibition is relieved through a poorly understood mechanism likely involving the disruption of an interaction between its CBD and the myosin head. Dissociation both frees the head to bind tightly to actin while exposing dimerization sites throughout the tail domain of myosin VI, allowing it to become a processive dimer (1, 105, 137).

Binding to members of either class of cargo protein is thought to relieve the auto-inhibition through the mechanism described above. Recently, however, myosin VI's activation mechanism has been found to be more elaborate, with evidence now showing that myosin VI binds specifically to the signaling lipid $PI(4,5)P_2$ as well as being activated using Ca^{2+} (**Figure 4**) (109, 136).

These outstanding questions on its activation mechanism, together with its many roles throughout the cell, make a method for controlling motor function with high spatial and temporal control particularly valuable for studying myosin VI. As discussed above, optogenetics provides an ideal approach to achieving this level of control. In the following section, I review the properties of myosin VI that make it an attractive target for optogenetic engineering.

1.3.4 The structure of the myosin VI cargo binding domain and its suitability for optogenetic control

To obtain light-controlled activation of myosin VI, we considered fusing a short peptide region of the myosin VI cargo protein Dab2 ($Dab2^{pep}$, res. 674-711) to the C-terminus of the LOV2 Jα helix. $Dab2^{pep}$ has been crystallized in complex with the cargo binding domain (CBD) of myosin VI (**Figure 5**), and has been shown to recruit the myosin VI tail *in vivo* (137). Phichith *et al*.

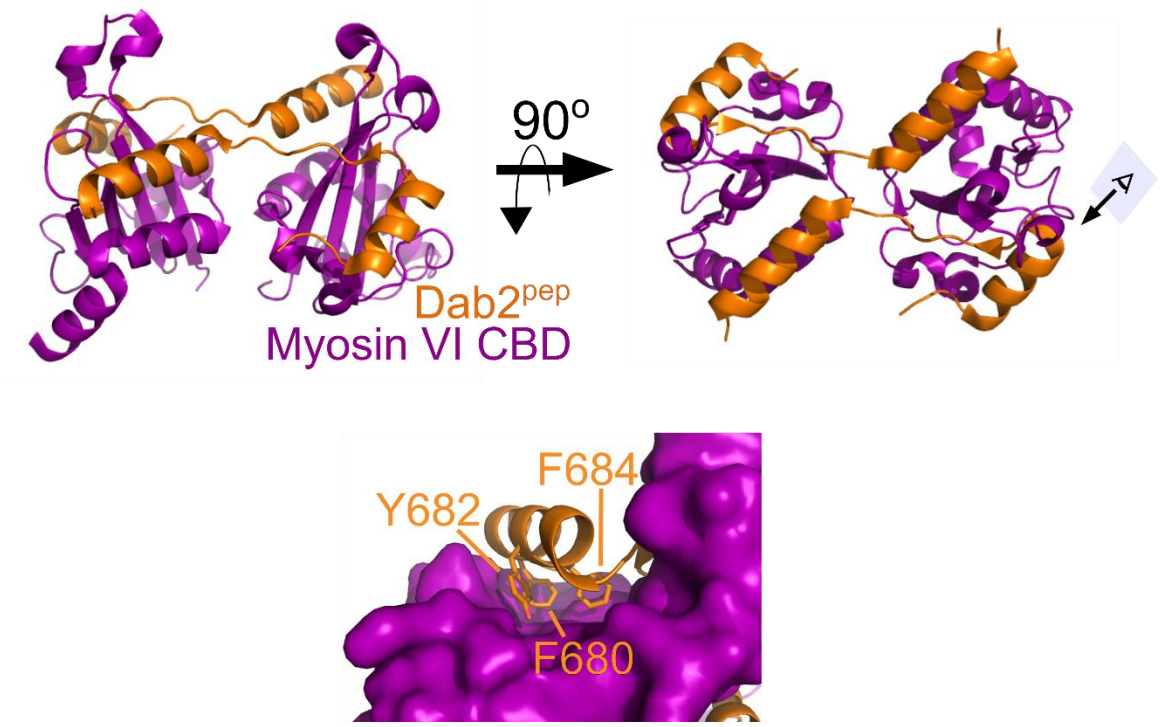

Figure 5. The myosin VI CBD and Dab2^{pep} co-crystal structure. *Top*: The myosin VI CBD co-crystalized with Dab2pep in two orientations illustrating how two Dab2pep molecules straddle the CBDs. *Bottom*: View of N-terminal Dab2^{pep}:CBD binding interface with aromatic residues shown in sticks. Viewing angle shown by eye in image on top right.

independently were able to activate full-length porcine myosin VI *in vitro* using high concentrations of a Dab2 truncation that included Dab2^{pep} (1). Additionally, ITC experiments suggest that the N-terminal α-helix of Dab2^{pep} contains most of its binding affinity for myosin VI, making Dab2^{pep} a suitable target for caging by the LOV2 domain.

In the crystal structure of the CBD-Dab2^{pep} complex, two CBDs and two Dab2^{pep} molecules form a tetrameric structure (**Figure 5**). Each Dab2^{pep} in the tetramer contains two helical regions that contact the CBDs. The two helices bind to opposite CBDs so that each Dab2^{pep} binds across both CBDs in the tetramer. The modest interface between the two CBDs in the tetramer suggests that the Dab2^{pep}s promote myosin VI dimerization by tethering two myosin VI molecules in close proximity to each other, disrupting the interaction of the CBD to the myosin VI head domain and promoting myosin VI dimerization at various sites along its tail domain (1, 105, 137). Whether Dab2^{pep} directly competes with the interaction between the CBD and the myosin VI head is not known. ITC measurements indicate that the majority of the binding affinity for the CBD lies in the N-terminal helix of each Dab2^{pep} (137). Taken together, these observations suggest that light-induced uncaging of the N-terminal region of two Dab2^{pep} peptides may be sufficient to control myosin VI dimerization. Furthermore, the 2:2 stoichiometry of the CBD_2:Dab2$^{pep}{}_2$ tetramer results in a binding reaction dependent on the square of the concentrationof Dab2^{pep}, which should amplify the switching capability of a LOV2-based optogenetic tool caging Dab2^{pep}.

Chapter 2

Recruitment and activation of myosin VI *in vivo*

2.1 LOVDab design and implementation in mitochondrial recruitment assay

To obtain light-controlled activation of myosin VI, we fused the portion of its cargo protein Dab2 (res. 674-711, $Dab2^{pep}$) that binds to the myosin VI cargo binding domain (CBD) to the C-terminus of the LOV2 Jα helix. Myosin VI cargo proteins tether myosin VI to membrane-bound organelles *in vivo.* Accordingly, we tested our designs using an assay that would recruit myosin VI to various membranes in the cell (**Figure 6A**). Mitochondria were an ideal first choice for such an assay since proteins can be targeted to the mitochondrial membrane by fusing the Tom70 transmembrane helix ($Tom70^{helix}$) to their N-termini (21). Additionally, myosin VI is not known to act on mitochondria, and overexpression of myosin VI in the cell should therefore not lead to increased background binding of myosin VI to this organelle. We thus cotransfected HeLa cells with $Tom70^{helix}$-Fluorescent Protein (FP)-LOVDab and -$LOVDab_{+ctrl}$ fusion proteins and full-length human myosin VI tagged with a complimentary FP on its N-terminus. Because the absorption λ_{max} of EGFP is similar to that of LOV2, we alternate which of two FPs, mCherry or EGFP, is on myosin VI and which is on LOVDab. The protein we intend to watch in both the light and the dark states of LOV2 is fused to mCherry in order to avoid simultaneous excitation of LOV2.

We first tested whether $Dab2^{pep}$ is sufficient to recruit full-length myosin VI using an uncaged, constitutively open fusion of $Dab2^{pep}$ to the C-terminus of the LOV2 Jα helix (**Figure 6B**). Residues 674-679 of $Dab2^{pep}$ are mostly glycine and serine, suggesting that these residues could serve as a flexible linker between the LOV2 domain and the remaining residues in

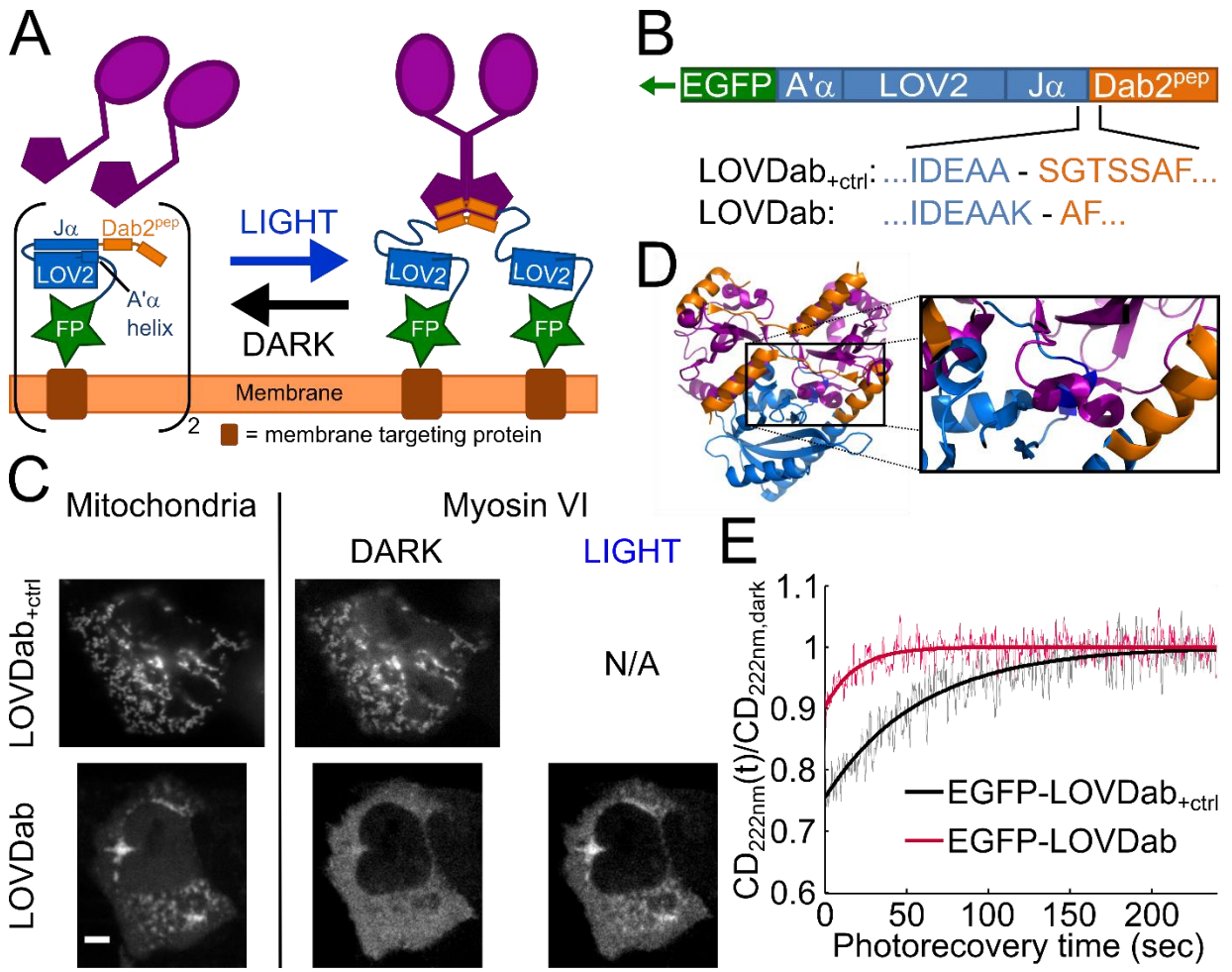

Figure 6. (**A**) Diagram of desired function of LOVDab. In the dark, Dab2^{pep} is prevented from binding myosin VI. When excited by blue light, the A'α and Jα helices of LOV2 unfold, releasing Dab2pep to recruit myosin VI to the membrane. An N-terminal tag targets LOVDab to a specific organelle in the cell. (**B**) Domain architecture of EGFP-LOVDab with the sequences of LOVDab$_{+ctrl}$ and LOVDab at the fusion site. (**C**) Recruitment assay from (**A**) performed using the constructs in (**B**). LOVDab$_{+ctrl}$ does not cage Dab2^{pep} in the dark whereas LOVDab only recruits myosin VI to the mitochondria in the lit state. Scale bar: 5 μm. (**D**) Alignment of LOV2 with Dab2^{pep}:CBD crystal structure (with zoom to boxed region on right) suggests LOVDab obstructs myosin VI binding to Dab2^{pep} in the dark. Dark blue: A'α helix. (**E**) Time course of dark state photorecovery of constructs in (**A**) measured by circular dichroism (CD) at 222nm normalized to their respective values in the dark state. At time = 0 sec the LOV2 domains are fully excited and allowed to recover in the dark.

Dab2^{pep}. This flexibility should prevent caging of the myosin VI binding site on Dab2^{pep} even when the Jα helix is folded in the dark. We refer to this construct as LOVDab$_{+ctrl}$ (**Figure 6B**). As expected, LOV2 fused to the full Dab2^{pep} sequence recruits myosin VI to mitochondria in the dark (**Figure 6C**). Myosin VI is seen on puncta that correspond to the mitochondria visualized in the LOVDab$_{+ctrl}$ channel. We refer to this construct as LOVDab$_{+ctrl}$ (**Figure 6B**), since it is always myosin VI binding-competent.

Having established that Dab2^{pep} is sufficient for myosin VI recruitment, we next sought to re-engineer LOVDab$_{+ctrl}$ to have light-dependent binding. Our strategy focuses on caging the aromatic residues F680, Y683, and F684 on the Dab2^{pep}'s N-terminal helix that are buried upon CBD binding (**Figure 5**, bottom). These three residues must be close enough to the Jα helix that they are sterically prevented from binding the CBD when the Jα helix is folded in the LOV2 dark state. This criterion is accomplished by reducing the number of intervening residues while maintaining a continuous helix encompassing the Jα helix and the N-terminal helix of Dab2^{pep}. An additional variable is helical registry which controls the relative orientation of the Jα and the Dab2^{pep} helices, and therefore the angle of the CBD-binding residues in Dab2^{pep} with respect to the LOV2 domain. Additionally, disruption of the interaction between I539 on the Jα helix and the LOV2 core partially unfolds the Jα helix (70). These constraints together limit the amount of Jα sequence we can modify.

We tested a small battery of constructs for light-dependent myosin VI binding using our mitochondrial recruitment assay (**Figure 6A**). One construct, which we refer to as LOVDab (**Figure 6B**), exhibits robust recruitment of myosin VI in response to light (**Figure 6C**). As intended, Tom70^{helix}-FP-LOVDab localizes to the surface of mitochondria, which are visible as puncta (**Figure 6C**). When the LOV2 is in the dark state, mCherry-myosin VI fluorescence

shows a diffuse, cytosolic signature indicating that it is unbound and diffuse throughout the cytosol. Upon LOV2 activation via whole cell illumination with a blue, 488 nm laser, the myosin VI fluorescence is depleted from the cytosol and forms puncta corresponding to the mitochondria where Tom70^{helix}-FP-LOVDab resides (**Figure 6C**). This indicates light-dependent binding between LOVDab and myosin VI.

Small deviations from this sequence abolish this light-dependent recruitment. LOVDab lacking K544 shows minor switching that was often accompanied with high dark state binding. LOVDab lacking both A543 and K544 shows weak, constitutive binding, indicating that moving the Dab2^{pep} closer to the LOV2 domain beyond these residues destabilized the Jα helix. The insertion of residues either C-terminal to K545 in the LOV2 sequence, or N-terminal to S678 in the LOVDab sequence, even when making compensatory insertions or deletions in the opposite fusion protein to maintain the myosin VI CBD binding site on the identical face of the Jα helix, prevents caging of Dab2^{pep}. Adding S678 of Dab2^{pep} to LOVDab produced a construct with similar switching as LOVDab. Following the predicted register of the helix, this fusion would position F680, a residue that is buried in the Dab2^{pep}:CBD interface (**Figure 5**), facing toward the Hβ-Iβ loop of LOV2. However, this construct shows a small level of dark state binding, so we continued our study with LOVDab.

Both LOVDab and LOVDab$_{+ctrl}$ contain the double mutation T406A/T407A on the A'α helix. This double mutation stabilizes the Jα helix by increasing the helicity of the neighboring A'α helix, which in turn improves caging of peptides fused to the Jα helix (21, 57). Modeling using the crystal structure of LOV2 and that of the Dab2$^{pep}{}_2$:CBD$_2$ complex suggests that LOVDab blocks Dab2^{pep} from binding to the CBD of myosin VI by sterically occluding the CBD from its binding site on Dab2^{pep} (**Figure 6D**). Interestingly, the largest steric clash is between the

CBD and the A'α helix, suggesting that both terminal helices contribute directly to the caging of Dab2^{pep}. In contrast, the flexible Dab2^{pep} residues 674-679 in LOV2Dab$^{pep}_{+ctrl}$ make this steric clash unlikely. This clash, together with the placement of Dab2^{pep} F680 in the LOV2 L546 position in LOVDab (55), may explain why this construct shows such robust light-dependent recruitment.

We further probed the structural changes in LOVDab and LOVDab$_{+ctrl}$ using circular dichroism (CD) at 222 nm to interrogate the light triggered unfolding of the Jα helix and the uncaging of Dab2^{pep}. In order to better replicate the protein used in the *in vivo* assays, we fused an EGFP to the N-termini of LOVDab and LOVDab$_{+ctrl}$ for our CD measurements. The observed 25% fractional change in helicity in EGFP-LOVDab$_{+ctrl}$ compares well with our previously measured values for the LOV2 domain (57), suggesting that fusion to either EGFP or Dab2^{pep} does not alter the extent of conformational change. We expect that Dab2^{pep} forms a helical extension of the Jα helix in LOVDab, whereas Dab2^{pep} is likely unfolded in EGFP-LOVDab$_{+ctrl}$, as Dab2^{pep}'s intrinsic helicity is only 0.64% (138). Consistent with this finding, the fractional change in helicity is smaller in EGFP-LOVDab than in EGFP-LOVDab$_{+ctrl}$ (**Figure 6E**), in part driven by the 20% higher intrinsic helicity of EGFP-LOVDab over EGFP-LOVDab$_{+ctrl}$. This decrease in apparent unfolding of the Jα helix supports the notion that the Dab2^{pep} is more tightly caged in LOVDab than in LOVDab$_{+ctrl}$.

2.2 LOVDab is a robust recruiter of myosin VI.

One benefit of optogenetic approaches is their ability to control proteins at a subcellular level. Using a focused laser beam, myosin VI recruitment via LOVDab was performed selectively on subcellular regions (<5 μm in diameter) in a reversible and repeatable manner (**Figures 7A-C**).

Overlaying the helix recovery CD trace of LOVDab on the mitochondrial fluorescence (**Figures 7C**) shows that myosin VI unbinds from the mitochondria at a similar rate to the Jα helix refolding in the dark, indicating that myosin VI recruitment is occurring through our LOV2 construct.

To test the generalizability of this recruitment, we targeted LOVDab to two other membranes, the plasma membrane. By fusing LOVDab to beta-2-adrenergic receptor (B2AR), we demonstrate recruitment of myosin VI to the plasma membrane in response to light (**Figures 7D,E**). The flat shape of the HeLa cell makes it more challenging to observe the contrast in cytosolic versus membrane-bound myosin VI as compared to that with mitochondria in the previous assay. Therefore, LOVDab is a robust recruiter of myosin VI.

2.3 Myosin VI recruits and activates myosin VI on peroxisomes.

2.3.1 Myosin VI is recruited to peroxisomes via Dab2^{pep}

Peroxisome movement is highly coupled to microtubule dynamics (139). Myosin V has previously been shown to slow the redistribution of peroxisomes upon recruitment of constitutively active kinesin-2, causing the peroxisomes to accumulate near the cell boundary. These observations suggest that myosins are capable of stalling and/or decoupling peroxisomes from microtubule machinery (140). We reasoned that if recruiting myosin VI to peroxisomes alters their motion inside the cell, this assay could determine whether LOVDab can activate myosin VI upon its recruitment. We targeted LOVDab and LOVDab$_{+ctrl}$ to peroxisomes by fusing the Pex3 membrane targeting domain (Pex3^{MTD}) to its N-terminus (141). We find that among cells co-transfected with Pex3^{MTD}-FP-LOV2Dab2$^{pep}_{+ctrl}$ and myosin VI, cells having high

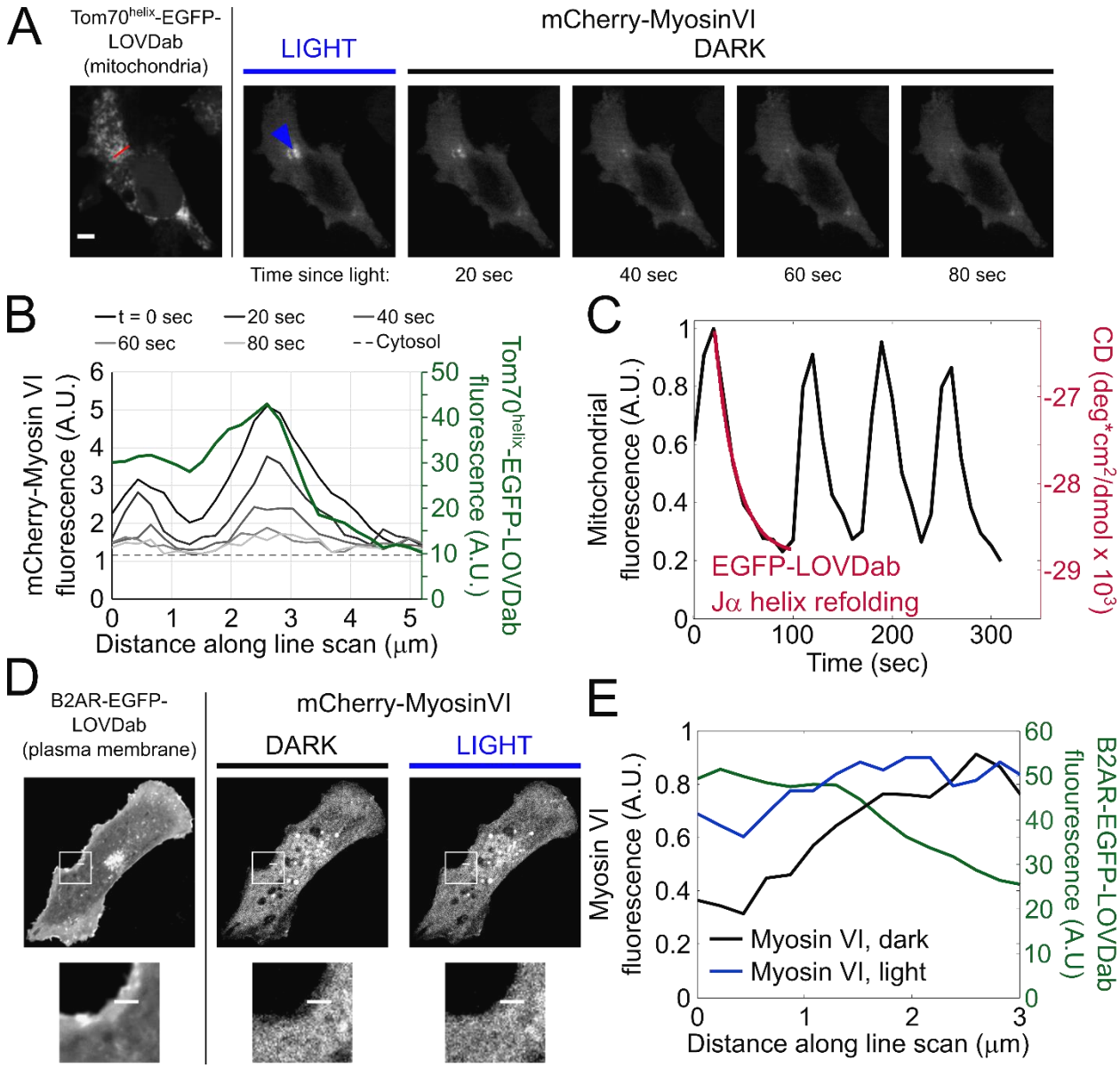

Figure 7. LOVDab robustly recruits myosin VI to different membranes within the cell in a light dependent manner. (**A-C**) Spot-specific, light-dependent recruitment of myosin VI to mitochondria. (**A**) Images of cell showing spot-dependent (blue arrow) recruitment of myosin VI. As cell is left in dark, myosin VI unbinds. Scale bar: 5 μm. (**B**) Fluorescence intensity line scan across red line in (**A**) over time. (**C**) Mean fluorescence in spot peak in (**A**) quantified over sequential pulses of light shows myosin VI recruitment is reversible and repeatable. Overlayed circular dichroism (CD) trace of EGFP-LOVDab photorecovery indicates that the myosin unbinding rate is similar to the refolding rate of the Jα helix in LOVDab. (**D**) Light-dependent recruitment of myosin VI to the plasma membrane. Bottom row: expanded view. Line is approximately 3 μm (see (**E**)). (**E**) Quantification of fluorescence of line in Panel (**D**). Fluorescence increases near cell edge where the plasma membrane is in focus.

myosin VI concentration exhibit constitutive binding between LOV2Dab2$^{pep}_{+ctrl}$ and myosin VI. In contrast, wild type peroxisomes do not show significant binding of myosin VI (**Figures 8A,B**).

We next targeted LOVDab to peroxisomes, and were able to achieve reversible, light-dependent recruitment of myosin VI to this organelle (**Figures 9A,B**). Furthermore, the recruitment occurs only to peroxisomes coated in LOVDab. Recruitment did not appear to be sufficient to deplete myosin VI from other vesicles in the cell, suggesting that our design does not impact native myosin VI activity.

2.3.2 Myosin VI stalls peroxisome movement

Significantly, peroxisomes that bind myosin VI have overall slower velocities than wild type peroxisomes, supporting previous data showing that myosin V is capable of stalling microtubule-directed transport of these organelles (**Figure 8C**) (140).

As light is applied to the cells, peroxisomes move more slowly. This is evident when projecting the maximum pixel values from consecutive blocks of 24-25 frames (46-48 seconds), as fast moving peroxisomes appear as blurred out clusters that coalesce into more defined, compact puncta in the light (**Figure 9C**). After three minutes in the dark, the peroxisomes return to being more mobile, as indicated by the diffuse puncta in the projections. We therefore conclude that LOVDab is capable of reversibly activating myosin VI *in vivo*.

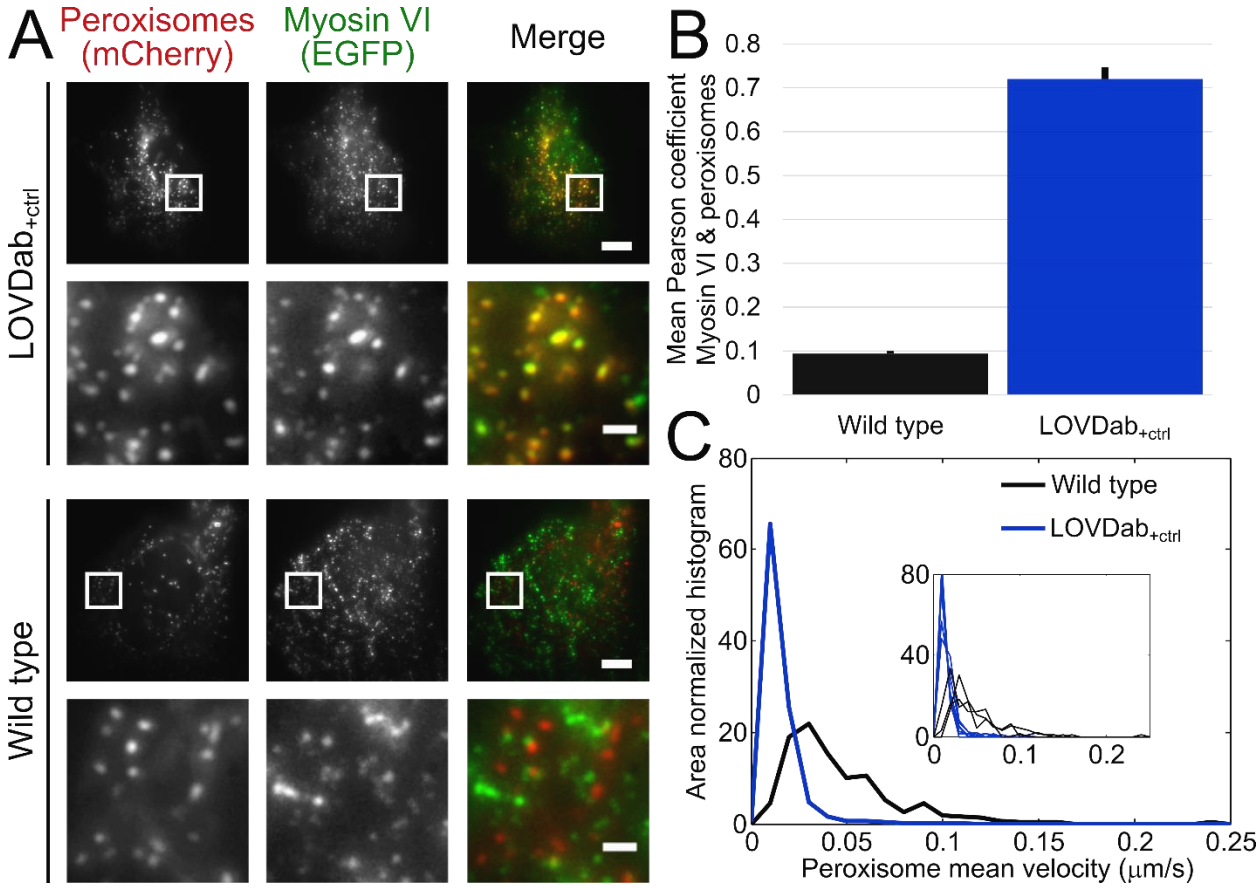

Figure 8. Myosin VI is recruited to peroxisomes via Dab2^{pep}. (**A**) The membrane targeting domain of Pex3 (Pex3^{MTD}) is used to express either mCherry-LOVDab$_{+ctrl}$ or mCherry only (Wild type). *Top two rows*: Cells with peroxisomes containing LOVDab$_{+ctrl}$ bind EGFP-myosin VI. *Bottom two rows*: Wild type peroxisomes lacking LOVDab$_{+ctrl}$ do not bind myosin VI. The 2nd and 4th rows are expanded views of boxed regions in the 1st and 3rd rows, respectively. Scale bars: 5 μm (1 μm expanded). (**B**) Quantification of overlap between peroxisome and myosin VI channels confirms significant recruitment of myosin VI to peroxisomes labeled with LOVDab$_{+ctrl}$ (mean ± SEM, p << .01, t-test; wild type, n=3; LOVDab$_{+ctrl}$, n=6). (**C**) Peroxisome frame-to-frame velocities are markedly reduced in cells expressing Pex3^{MTD}-mCherry-LOVDab$_{+ctrl}$. Inset shows distributions for each cell used in analysis. Main graph shows distributions pooling all peroxisome data from these cells.

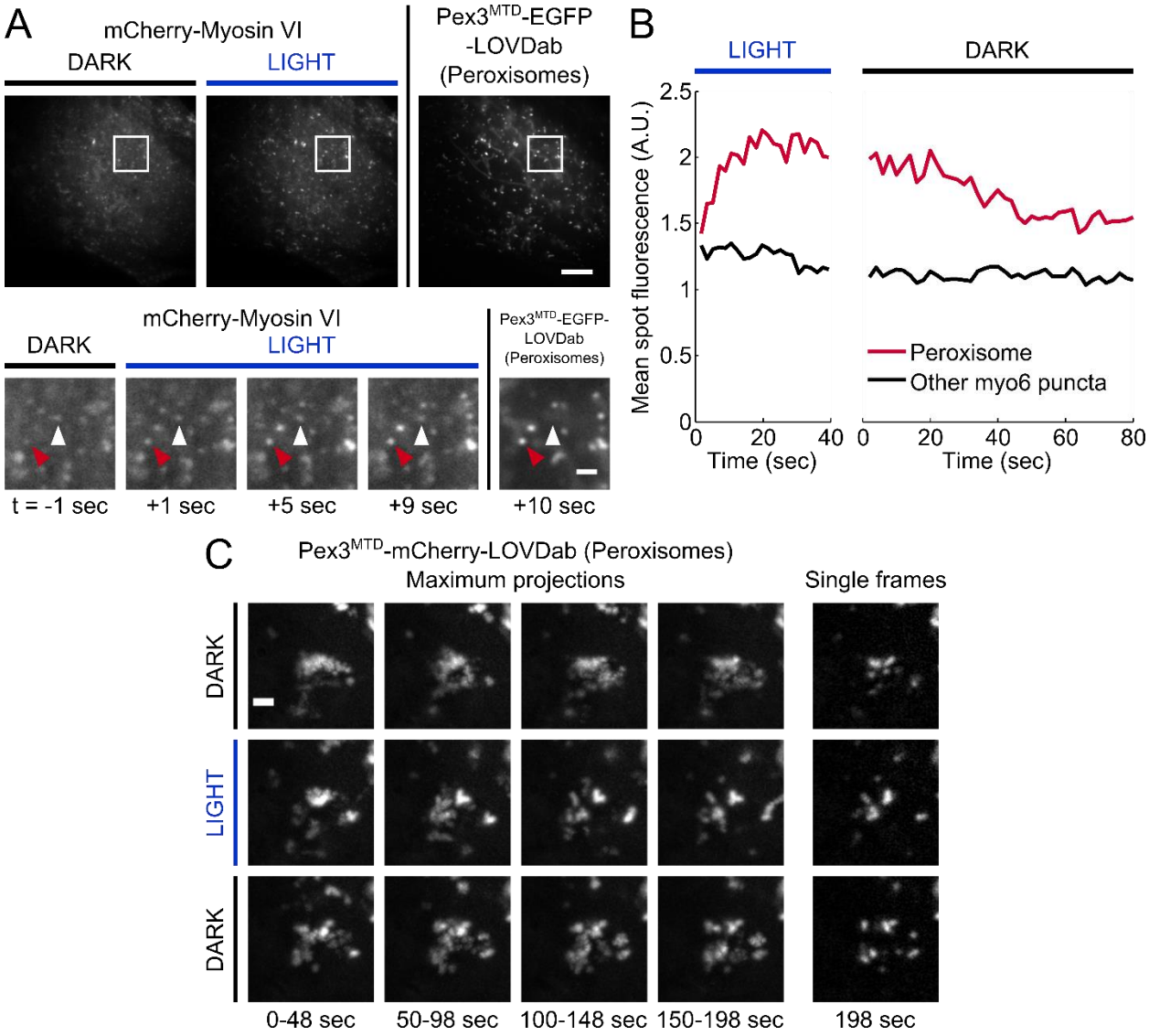

Figure 9. LOVDab reversibly recruits EGFP-myosin VI to peroxisomes in a light-dependent manner, which causes them to stall. (**A**) Images of cell showing light-dependent recruitment of myosin VI to peroxisomes. *Top row*: whole cell view. *Bottom row*: expanded image of boxed region. Vesicles showing light-dependent recruitment (red arrows) correspond to peroxisomes (right image) while vesicles binding myosin VI in the dark do not (white arrows). Thus, light-dependent recruitment occurs through LOVDab. Scale bars: 5 μm (1 μm expanded). (**B**) Quantification of fluorescence of vesicles labelled in (**A**). The red line corresponds to red arrowed vesicle; black line to the white labeled vesicle. (**C**) Maximum intensity projections over 48-50 seconds of peroxisome movement in a cell expressing EGFP-myosin VI and Pex3^{MTD}-mCherry-LOVDab. Peroxisomes moving diffusively appear blurred out and occupy expanded areas. Restricted peroxisomes occupy compact spaces (see right picture, middle row). As LOVDab is activated, peroxisomes stall, displaying more limited excursions. Motions resume after peroxisomes are left in the dark (3 minute delay between middle and bottom row). Projections constructed from consecutive blocks of 24-25 two second frames. Each row is from separate video; time increases down and to the right. Scale bar, 1μm.

2.4 Discussion of results and implications.

Myosin VI is the only myosin that walks toward the pointed end of actin filaments (7, 8). This property gives it many different roles throughout the cell including endocytosis, cell migration, and autophagy (122). Furthermore, the mechanism for myosin VI activation is still highly constitutively active, truncated, forced-dimer motor proteins (142, 143). These designs provide an excellent means of laser-induced force-generation *in vivo*, and allow researchers to use members of each of the three classes of motor proteins. LOVDab differs in that it controls myosin VI through its native activation mechanism without any alterations to the myosin itself. Thus, our approach allows for direct tests of myosin VI function and control in cellular contexts. Additionally, since full-length myosin VI is auto-inhibited when not bound to cargo, our method couples recruitment and motor activity, preventing potential adverse effects on cytoskeletal systems when myosin VI is expressed *in vivo*.

Curiously, LOVDab places the residue F680 of $Dab2^{pep}$ (res. 674-711) in the L546 position of LOV2, which Guntas *et al* observed to bind to a hydrophobic pocket in the non-FMN binding face of the β sheet of LOV2 (55). When optimizing their LOV2-based recruitment system, "improved Light Inducible Dimer (iLID)", they noticed their optimal switch had a key phenylalanine residue that bound this pocket. Another parallel between our designs is a shortened photorecovery time. Their optimal construct exhibits a photorecovery time with $\tau \approx 22$ seconds relative to the wild type value of 80 seconds (57). Similarly, LOVDab exhibits a $\tau = 15$ seconds compared to $LOVDab_{+ctrl}$ which has a mean $\tau = 47$ seconds, much closer to the recorded value for LOV2 406A/407A of 56 seconds (67). The relative difference in photorecovery times are evident from the rates of Jα helix reversion in **Figure 6C**. Given the relative intolerance of LOVDab to deviations of F680 from this position, these results suggest that this hydrophobic

pocket may be of general importance for caging peptides on the C-terminus of LOV2. Furthermore, a quickened dark state reversion time may highlight a key role of the L546 pocket in the overall conformational dynamics of the LOV2 domain. In any case, it seems that placing the Dab2^{pep} F680 in this pocket contributed to robust, light-dependent recruitment of myosin VI by LOVDab.

We demonstrated that LOVDab is capable of recruiting myosin VI in a light-dependent manner to mitochondrial, plasma, Golgi and peroxisomal membranes. Strictly speaking, however, binding of myosin VI to Dab2^{pep} is not equivalent to activation. Activation requires the release of autoinhibition of full-length myosin VI, allowing it to interact with actin in either a transport (124) or anchoring role (126). In order to demonstrate activation of myosin VI *in vivo*, we showed that myosin VI recruited to peroxisomes via our engineered positive control construct LOVDab$_{+ctrl}$ stalls these organelles. Similarly, upon activation with light, LOVDab reversibly recruits myosin VI at high concentrations in the cell, stalling peroxisomes. These findings indicate that upon recruitment by LOVDab, myosin VI is capable of interacting with actin strongly enough to decouple peroxisomal motion from the underlying microtubule-based processes that drive their native behavior (139). This strongly suggests that LOVDab is capable of activating myosin VI *in vivo*.

2.5 Materials and Methods

Plasmid construction

For protein purification, plasmids encoding LOV2-Dab2^{pep} fusion proteins were engineered within a pHISparallel1 vector encoding a modular -/NdeI/-His6-Protein G-/AgeI/-EGFP-/EcoRI/-LOV2-Dab2^{pep}-/XhoI/- that allowed for facile swapping of domains via ligation.

For live cell imaging, LOV2-Dab2^{pep} plasmid constructs were created for transfection using ligations from a modular pEGFP vector containing the general sequence -/NheI/-membrane tag-/AgeI/-FP-/EcoRI/-LOV2-Dab2^{pep}-/BamHI/- Membrane tags include: for mitochondria, the mitochondrial outer membrane targeting sequence of yeast Tom70^{helix} (res. 1-40); for the plasma membrane, full length golden hamster Beta-2-Adrenergic Receptor (B2AR); for the Golgi Apparatus, full-length human KDEL receptor containing a R5Q/D193N double mutation to improve retention in the Golgi (144, 145); and for peroxisomes, the N-terminal targeting sequence of human Pex3 (res. 1-42) (Pex3^{MTD}) with a (GGS)x3 linker (141, 146). Tom70^{helix} and B2AR were generous gifts from M. Glotzer. KDELR and Pex3^{MTD} were constructed from gBlocks ordered from Integrated DNA Technologies (Coralville, IA). Full-length human myosin VI, isoform 1 (a generous gift from M. Zhang) was expressed in their modified pET vector containing a sequence encoding -/NheI/-FP-/XhoI/-myosin VI-/NotI/-. Fluorescent proteins were exchanged via ligation.

Live cell assays

HeLa cells were passaged in Dulbecco's modified Eagle medium (DMEM) from Corning (New York, USA) supplemented with 10% heat-inactivated FBS (Sigma, Missouri, USA) and 1x HyClone penn-strep-L-glut (GE Healthcare Life Sciences, Utah, USA). One day prior to transfection, cells were split onto plasma cleaned glass coverslips. Coverslips that were 80-95% confluent were washed into DMEM media lacking supplements 10-20 minutes prior to transfection. Cells were co-transfected with a combination of plasmids containing genes for either an FP-LOV2-Dab2^{pep} construct fused to a gene encoding an organelle-targeting transmembrane protein at its 5' end or a gene encoding full-length human myosin VI with either

EGFP or mCherry2B (see above) at its N-terminus using Lipofectamine 2000 (Life Technologies, Illinois, USA), according to the manufacturer's guidelines. Cells were imaged 18-24 hours post-transfection. Confocal images were taken using a 63×, 1.4 numerical aperture (NA) objective on an Axiovert 200M microscope (Zeiss) with a spinning disk confocal (CSU10, Yokogawa) and an electron-multiplying charge-coupled device (EMCCD) camera (Cascade 512B, Photometrics). The microscope was controlled using MetaMorph (Molecular Devices). TIRF images (peroxisome experiments) were taken using the microscope used in the gliding filament assay. Videos were background subtracted using either the rolling ball or parabolic algorithms in ImageJ (147). Quantified pixel values are plotted post-background subtraction to match images shown.

EGFP-LOV2Dab2^{pep} purification and spectroscopy

LOV2-containing constructs were purified as described previously (57). Briefly, constructs were expressed in E. coli with an $(His)_6$-Protein G fusion to their N-terminus, followed by a TEV protease restriction site. After elution from the Ni-NTA column, proteins were dialyzed against a TEV protease cleavage buffer (50 mM Tris, 1 mM EDTA, 1 mM DTT, pH = 8.0) before or during the cleavage reaction. EDTA and DTT were removed by dialysis prior to passing the cleaved protein through a regenerated Ni-NTA column. Proteins were then concentrated and ran on a size exclusion column (HiPrep 16/60 S-100 HR, GE Healthcare Life Sciences) that was equilibrated in the relevant assay buffer.

Protein purity was assessed using SDS-PAGE. In the case of LOV2-containing constructs, protein quality was further assessed using UV-Vis spectroscopy to measure the FMN photorecovery rate and circular dichroism (CD) (see below) to measure the fractional change in

helicity of the protein, as done previously in our lab (57). The UV-Vis spectroscopy was carried out on an Olis HP 8452 Diode Array Spectrophotometer (Bogart, GA). The recovery of FMN absorbance at 448 nm was fit to a single exponential using MATLAB to obtain the FMN dark state recovery time constant, τ_{FMN}. Circular dichroism (CD) was performed on a Jasco 715 spectrophotometer and a 40W white LED lamp (BT DWNLT A, TheLEDLight.com) was used to excite the LOV2 domain in the cuvette for $\geq$ 12 seconds for photo excitation. The refolding traces at 222 nm were fit to a single exponential using MATLAB and the fractional change in helicity in the protein as $\delta_{222} = (CD_{222,dark}-CD_{222,light})/CD_{222,dark}$.

Chapter 3

Purification and activation of myosin VI in *in vitro* gliding filament assay

3.1 Titer assay optimization

Myosin VI could theoretically halt peroxisome movements by binding to actin filaments either with or without motor activity. We therefore wanted to purify myosin VI and directly test its activation by LOVDab *in vitro*. Myosin VI did not express well enough to warrant a transfection-based protocol, so I sought out a means of myosin VI expression using a baculovirus system. The details of making the P0 virus are included in **Section 3.5** below. Myosin VI expression required that we titer the virus to obtain a precise multiplicity of infection (MOI), which is the ratio of the number of infectious units of a virus to the number of host cells it is added to. We find that an MOI of one works best for myosin VI. In order to calculate the optimal MOI, we had to first optimize a way to determine the concentration of infectious units in our viral preps, or the viral titer. To do this, I needed to optimize the titer assay for our virus.

The core strategy of any titer assay is to dilute the virus until single infection events can be counted. Then the fraction of infection events that occur at each dilution are used to calculate the titer that would most likely yield those same probabilities of infection. Since the estimate of the fraction infected is more accurate at higher sample numbers, a 96-well plate format is desirable in order to get large numbers of infection samples with minimal resource consumption.

Our baculovirus includes the *lacZ* gene so that the virus can be titered using the ability of LacZ to convert the chemical X-gal, which is colorless, to 5,5'-dibromo-4,4'-dichloro-indigo, which is blue. Unfortunately, X-gal is only stable in water for a couple days at room temperature, whereas it can take 6-7 days to produce the LacZ protein in infected SF9 cells. An additional challenge with this format is that it is difficult to exchange the cell media in the 96 wells, and

doing so risks cross-well contamination. By testing different conditions, I found that plating the SF9 cells at low density (0.5x10^6/mL) and waiting 6 days prior to adding the X-gal to the wells overcame these issues. I recorded which wells are colored on the following day. Infecting SF9 cells at an MOI of one using the titer values calculated in this way allowed me to perform the experiments described below.

3.2 TIRF gliding filament assay shows LOVDab is capable of activating myosin VI

3.2.1 Demonstration of light-dependent activation with low [KCl] myosin VI

In order to directly demonstrate activation of myosin VI motility by Dab2^{pep}, we designed a modified gliding filament assay whereby we anchor an EGFP-LOV2-Dab2^{pep} fusion protein to the surface of a glass coverslip through an anti-GFP antibody (3E6). We then perfuse soluble mCherry-myosin VI with actin together (**Figure 10A**). This design allows us to interrogate myosin VI activation without altering its C-terminal cargo binding domain.

We find that full-length human myosin VI purified in a low salt ([KCl] = 25mM) MOPS buffer propels filaments at approximately 170 nm/sec when recruited by LOVDab$_{+ctrl}$. This velocity agrees well with published values (148, 149). Under these conditions, LOVDab$_{+ctrl}$ recruits actin to the surface rapidly in the dark (**Figure 10B**, lower panels).

When the coverslip is coated with LOVDab, myosin VI only recruits actin to the surface after LOV2 is excited with blue light (**Figure 10B**). After 400 seconds of excitation, the coverslip surface is not yet saturated with actin, indicating that the actin deposits at a slower rate than with LOVDab$_{+ctrl}$-coated coverslips. The velocity of the actin filaments recruited through LOVDab is similar to that of filaments recruited through LOVDab$_{+ctrl}$ (**Figure 10C**). This latter

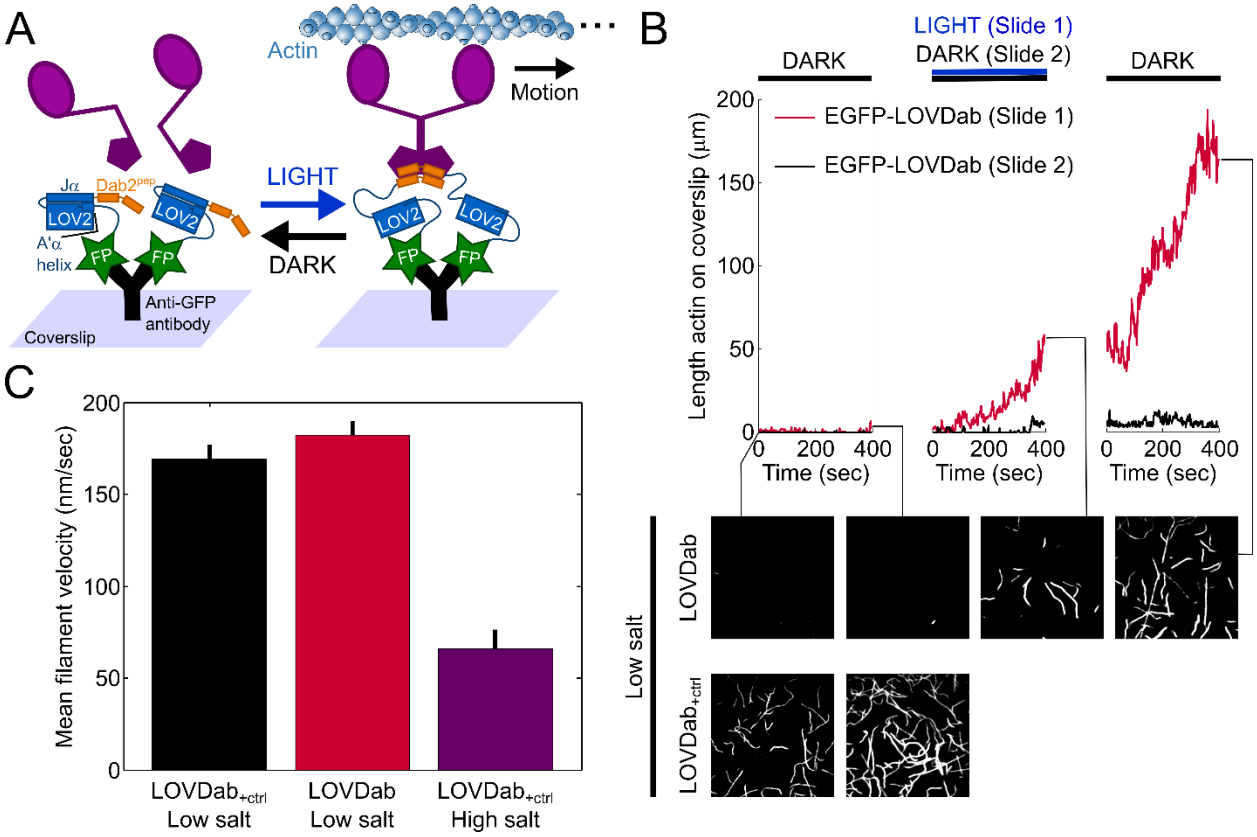

Figure 10. *In vitro* gliding filament assay indicates that LOVDab activates full-length human myosin VI in response to light. (**A**) Diagram of the modified gliding filament assay. EGFP-LOVDab is attached to the coverslip surface using an anti-GFP antibody. Soluble myosin VI is recruited to the surface by $Dab2^{pep}$ and translates actin filaments. (**B**) Quantification of actin binding to surface over time for LOVDab. Recorded in multiple videos. Slide 1 was prepared and excited throughout second video. Slide 2 was left in the dark for all three recordings. Pictures underneath correspond to indicated time points in red curve. Below, matching time points for a representative slide coated with $LOVDab_{+ctrl}$ are included for comparison. (**C**) Filament velocities in different conditions. Salt significantly alters filament velocity while velocities for LOVDab and $LOVDab_{+ctrl}$ are similar (mean + SEM; first column, n=4; others, n=3).

finding suggests that both constructs fully activate myosin VI. The slower deposition rate for LOVDab may be due to the lower availability of the $Dab2^{pep}$ in LOVDab over $LOVDab_{+ctrl}$, leading to fewer recruited myosin VI motors. It could also reflect the selective recruitment of microaggregates of myosin VI by LOVDab, which would diffuse to the surface more slowly than monomeric myosin VI (see below).

For both constructs, myosin VI appeared to be recruited to the surface irreversibly, as once the LOV2 was activated, actin did not unbind from the slide (**Figure 10B**, lower panels). In order to determine whether this irreversibility was due to the high affinity of $Dab2^{pep}$ for the myosin VI CBD, we inverted the gliding filament assay in order to observe myosin VI directly walking on actin. However, upon doing so we found that myosin VI purified in low salt solutions formed soluble microaggregates which we could observe in the TIRF microscope.

3.2.2 Re-optimization of myosin VI purification

The original myosin VI prep had three buffers: lysis, wash, and storage/assay (see section 3.5 for recipes). However, the original storage/assay buffer contained imidazole, which catalyzes the dark state reversion reaction for LOV2 (150). We therefore modified the protocol so that MOPS was the buffering salt, which is commonly used in myosin motility assay buffers (151, 152).

Upon discovering microaggregates in these preps, we sought to re-optimize our myosin VI purification protocol to improve myosin VI solubility. It soon became apparent that sampling a significant number of different buffer conditions was intractable if three buffers were to be considered. In order to impose consistency in the search, and drastically reduce the number of conditions to be tested, I chose to move forward with a single buffer preparation where the lysis,

wash, and storage buffers differed only in whether they contained the membrane-disrupting detergent triton-X100 plus protease inhibitors, protease inhibitors only, or neither, respectively.

I varied the identity of the buffer salt, the ionic strength of the buffer through KCl concentration, and pH. The primary tests for determining whether a myosin VI preparation was successful were measuring the amount of protein in the preparation by SDS-PAGE, and to test that washing out free myosin and actin would release actin from the surface in a gliding filament assay after myosin VI and actin were recruited to the coverslip via LOVDab$_{+ctrl}$. I found that a buffer with 50 mM Tris-HCl, 150 KCl, pH=7.3 performed best. Changing any of these factors to their value in the original prep condition decreased the protein yield, or caused the myosin VI recruitment to the coverslip to be irreversible. I call this buffer the "high salt" buffer.

3.2.3 LOVDab$_{+ctrl}$ activates myosin VI prepared in high salt

Myosin VI prepared in a high salt (KCl = 150 mM) Tris buffer did not form visible microaggregates, and was active in the gliding filament assay when LOVDab$_{+ctrl}$ was on the surface. Consistent with a reduction in the myosin:actin affinity in high salt, filaments recruited to the surface in this assay had a significantly reduced velocity (**Figure 10C**). This myosin also did not perform in the TIRF assay, either because the concentration needed to dimerize the myosin VI using cargo was prohibitively high for detection using TIRF, or because of the well-documented decrease in affinity between myosins and actin in high KCl conditions (153, 154).

Unlike in low salt conditions, the washing out of free actin and myosin VI from the slide results in the slow unbinding of myosin VI from LOVDab$_{+ctrl}$. (**Figure 11**) Together, the high off-rate of the myosin VI from the mitochondria and the reversibility in the high salt myosin VI preparation suggest that the irreversibility seen in the gliding filament assays using myosin VI

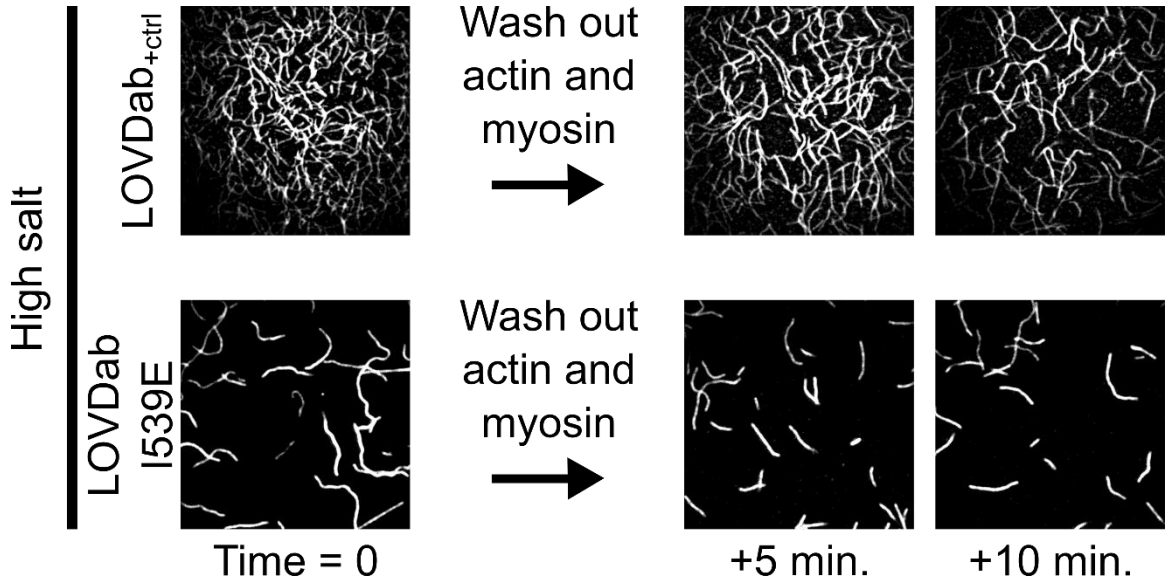

Figure 11. Myosin VI purified in high salt binds actin reversibly and is recruited by LOVDab. *Upper row*: in high salt, actin releases from coverslip when free myosin and actin are washed out of the slide. *Lower row*: the I539E mutation unfolds the Jα helix, acting as a constitutive lit state mutant. This mutation allows LOVDab to recruit actin to the surface in high salt.

prepared in low salt was primarily due to the presence of myosin VI microaggregates. However, without the high avidity of the myosin VI microaggregates, we did not observe recruitment of actin to the surface via LOVDab under high salt conditions. In some instances, if we concentrated the myosin in high salt and diluted into low salt, we observed weak recruitment of actin to the surface, but in a light-independent manner. We therefore postulate that this recruitment was due to deposition of myosin VI directly onto the coverglass after it was diluted into a buffer in which it is insoluble. Given that myosin VI prepared in high salt is active when recruited through LOVDab$_{+ctrl}$, we postulate that the lack of observance of myosin VI recruitment to LOVDab *in vitro* is due to the engineered caging effect of the LOV2 domain on Dab2^{pep} in the LOVDab construct. This effect could weaken the effective K_D for binding of Dab2^{pep} to myosin VI to a point where even in the light, the myosin VI could not be recruited at concentrations where it is soluble in our high salt buffers.

However, a lack of actin recruited to the surface does not necessarily mean that myosin VI is not being bound by Dab2^{pep}. In the model where myosin VI must dimerize in order to transport cargo, the lack of actin on the surface may indicate that myosin VI recruitment is rare or short lived enough that dimers cannot form or exist long enough for actin to touchdown in the same place on the coverslip, rather than an inability to bind myosin VI. Importantly, LOVDab containing an I539E point mutation constitutively recruited actin in the presence of high salt myosin VI, proving that LOVDab is inherently capable of activating myosin VI (**Figure 11**).

We also tested whether a LOV2 domain fused to the myosin VI-binding residues (412-520) of optineurin (OPTN) could activate myosin VI in our gliding filament assay. Though EGFP-LOV2-OPTN$_{(412-520)}$ migrates as a dimer in size exclusion chromatography (**Figure 12**), it does not activate myosin VI. Lack of activation is consistent with recent studies showing that the large

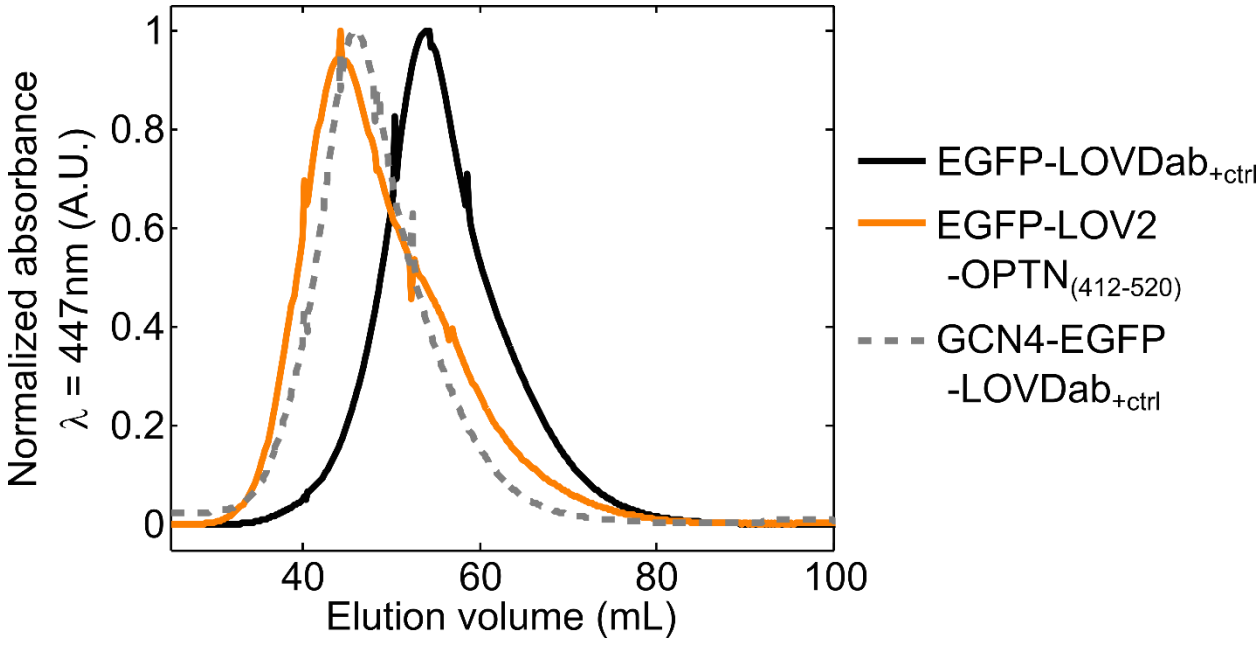

Figure 12. EGFP-LOV2 fused to the myosin VI-binding portion of Optineurin migrates as a dimer by size exclusion chromatography. Optineurin (OPTN) has previously been shown to activate full-length porcine myosin VI at much lower concentrations than a truncated portion of Dab2 containing $Dab2^{pep}$ (1). We therefore wanted to test whether the putative myosin VI binding site on OPTN (res. 412-520) could activate full-length human myosin VI in our gliding filament assay. Comparison to the elution trace of $EGFP\text{-}LOVDab_{+ctrl}$ dimerized via a GCN4 leucine zipper, $OPTN_{(421\text{-}520)}$ fused to the C-terminus of EGFP-LOV2 migrates as a dimer in our size exclusion column. This is consistent with previous reports showing OPTN is a dimer (1) and the prediction that these residues in OPTN form a coiled-coil (2, 3). However, EGFP-LOV2-$OPTN_{(412\text{-}520)}$ did not recruit actin to the surface of our gliding filament assay, seemingly inconsistent with the study showing activation of porcine myosin VI via optineurin. (1). Though OPTN binding to the myosin VI tail was shown to be large insert independent (13), one difference between porcine myosin VI and our human full length construct is that our construct contains the large insert of isoform 1. Since doing this experiment, a group of researchers have shown that myosin VI binds OPTN only after it has been ubiquitinated (14), and have solved the structure of a molecular "switch" region in the tail domain involving the long insert that occludes the OPTN binding site (15). Our results therefore support their findings.

insert in the myosin VI tail domain, which is present in our construct, occludes the OPTN binding site (15). Furthermore, OPTN must be ubiquitinated prior to binding myosin VI (14).

In summary, we have demonstrated that both LOVDab and LOVDab$_{+ctrl}$ are capable of directly of activating myosin VI, supporting our claim that the stalling of peroxisomes upon recruitment of myosin VI is due to activated myosin VI resisting the MT-directed transport of these vesicles.

3.3 Evidence that myosin VI integrates cargo signals

3.3.1 Sensitization of myosin VI to protein cargo using PI(4,5)P_2

Other factors that may contribute to the differences in our *in vivo* and *in vitro* assays include the lack of Ca^{2+} and PI(4,5)P_2 in the *in vitro* assays, both of which are known to bind myosin VI (109, 136). At myosin VI concentrations too low to interact with LOVDab$_{+ctrl}$, the addition of PI(4,5)P_2 rescued recruitment of actin to the coverslip (**Figure 13**). This effect required the presence of Ca^{2+} ions, suggesting that the three signals, PI(4,5)P_2, Ca^{2+}, and Dab2, are integrated to activate myosin VI in the proper time and place in the cell. The presence of these signals *in vivo* also may rationalize why myosin VI is activated by LOVDab *in vivo* but not in our *in vitro* gliding filament assay.

3.3.2 Myosin VI recruitment to the Golgi is uncorrelated with the amount of LOVDab on the membrane.

We realized that our results showing sensitization of myosin VI to protein cargo via lipid binding could explain results we had seen targeting LOVDab to the Golgi using the KDEL receptor (KDELR). Overexpression of KDELR seems to be cytotoxic. However, at low expression levels

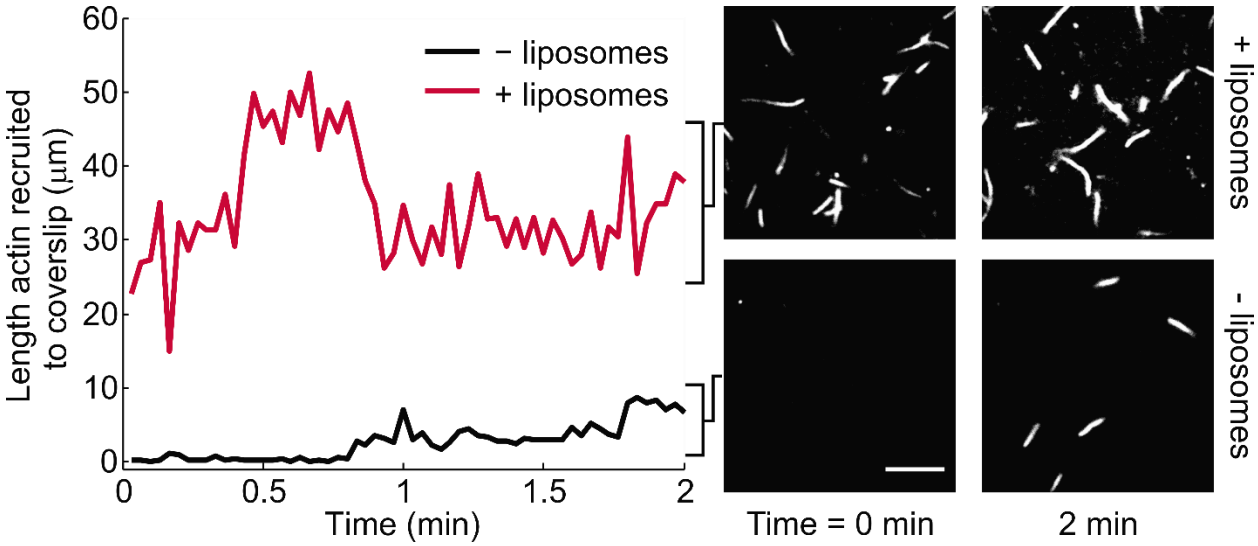

Figure 13. Lipid cargo sensitizes myosin VI to protein cargo Dab2^{pep}. At concentrations of mCherry2B-Myosin VI (prepared in physiological KCl conditions, see text) too low for LOVDab$_{+ctrl}$ to recruit actin to the coverslip (- liposomes, bottom), addition of artificial liposomes containing 5% PI(4,5)P_2 sensitizes full-length myosin VI to Dab2^{pep} cargo, rescuing recruitment of actin to the surface (+ liposomes, top).

KDELR-FP-LOVDab recruits myosin VI to the Golgi apparatus in a light-dependent manner (**Figure 14A,B**).

Notably, the amount of myosin VI binding to each LOVDab-labelled membrane does not correlate with the amount of LOVDab on that membrane (**Figure 14C**). This is especially apparent in the peripheral stacks of Golgi (**Figures 14A,B**). A lack of correlation could be detected at limiting myosin VI conditions where LOVDab is in vast excess over the myosin. However, the optogenetic nature of LOVDab allows us to interrogate the myosin:Dab2^{pep} interaction at two effective Dab2^{pep} concentrations. Since the lack of correlation persists in both the light and the dark, and additional myosin VI binding occurs in the light, the lack of correlation cannot be explained by limiting myosin VI. This means that other factors on these membranes must alter the myosin VI affinity for its protein cargo Dab2^{pep}, even between similar membranes in the same cell.

Together, these data support a new model of myosin VI activation whereby myosin VI integrates multiple cargo signals to deploy in a site-specific manner in the cell (**Figure 15**, see discussion below). The presence of these signals *in vivo* also may explain why myosin VI is activated by LOVDab *in vivo* but not in our *in vitro* gliding filament assay.

3.4 Discussion of results and implications.

In order to verify activation of myosin VI directly, we developed a modified *in vitro* gliding filament assay in which myosin VI is recruited to the coverslip via LOVDab or LOVDab$_{+ctrl}$. Myosin VI purified under either high or low salt conditions is active when recruited through LOVDab$_{+ctrl}$. Moreover, at low concentrations of myosin VI, PI(4,5)P_2 -containing liposomes

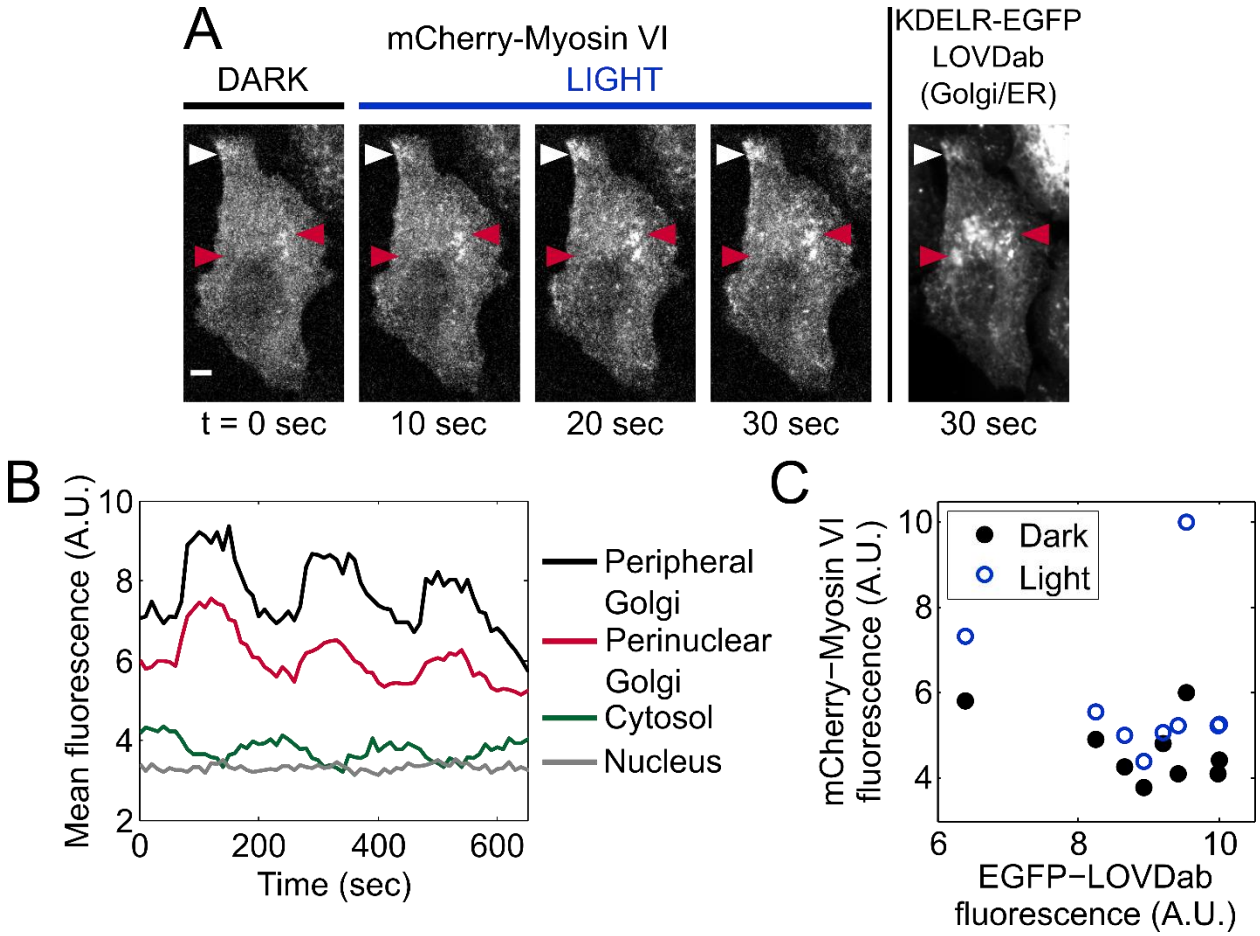

Figure 14. Myosin VI integrates cargo signals when recruited to the Golgi. (**A**) LOVDab was targeted to the Golgi apparatus using a KDEL receptor (KDELR) with an R5Q/D193N double mutation to promote retention in the Golgi. White arrows highlight peripheral Golgi that exceptionally recruits myosin VI. Red arrows highlight portions of perinuclear Golgi stacks, some of which recruit myosin VI well (right arrow) whereas others have minor switching (left arrow). Scale bar: 5μm. (**B**) Mean fluorescence in different areas of the cell described in (**A**) Perinuclear Golgi fluorescence is the mean of all perinuclear stacks. Cytosolic fluorescence is anticorrelated with Golgi fluorescence, indicating depletion of myosin VI from the cytosol upon excitation of LOVDab. Nuclear fluorescence is static and indicates the noise level of the measurement. (**C**) The amount of myosin VI binding is not correlated with the amount of LOVDab on the different Golgi stacks, indicating other factors in the cell must alter the myosin VI:LOVDab affinity on the different membranes.

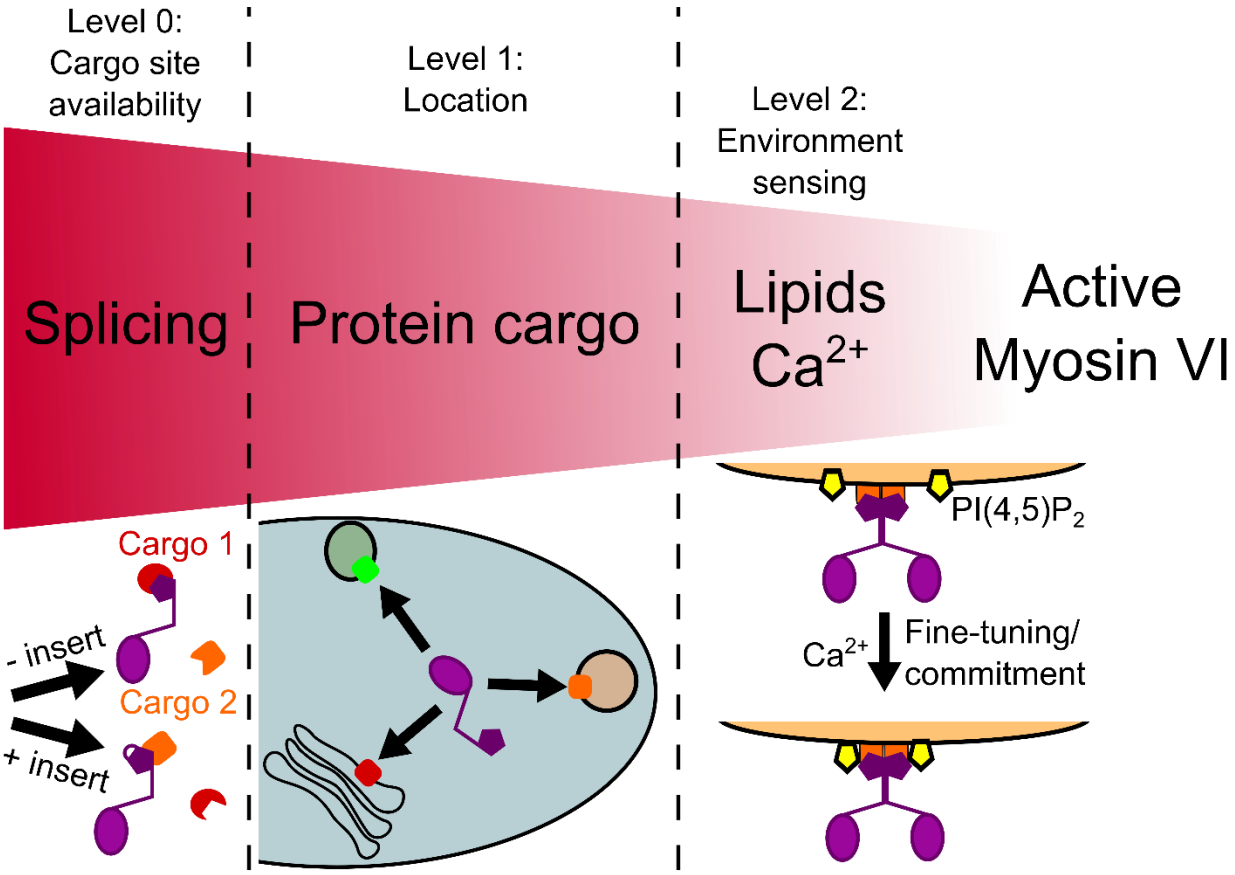

Figure 15. Model of myosin VI cargo integration in the cell. Alternative splicing biases myosin VI isoforms to different cargo proteins. Protein cargo recruits myosin VI isoforms to specific locations in the cell and determines its oligomeric state. Lipid, Ca^{2+}, and other cargoes help myosin VI sense the environment, modulating its affinity for cargo, as seen in (**Figures 13,14**).

enhance myosin VI's affinity for LOVDab$_{+ctrl}$ (**Figure 13**). This suggests that lipid binding at the plasma membrane, which is enriched in PI(4,5)P_2 (155), enhances myosin VI's effective affinity to its cargo protein Dab2^{pep}. This enhancement requires Ca^{2+}, supporting recent studies suggesting that Ca^{2+} transients could play a role in regulating myosin VI function (109, 136).

Moreover, when LOVDab is targeted to the Golgi apparatus, the amount of myosin VI bound does not scale with the amount of LOVDab on a given stack. This indicates that differences in these organelles alter myosin VI's affinity for its protein cargo. One cause for this difference could be in the concentrations of PI4P on the different stacks. Though myosin VI binds more strongly to PI(4,5)P_2, it also shows significant binding to PI4P (136), which is found on the Golgi (155). Another source of diversity is likely in Ca^{2+} transients, as organelles in the secretory pathway, including the Golgi, are rich in Ca^{2+} (156). The cisternae in the Golgi have different luminal Ca^{2+} concentrations based on their developmental stage and differentially release Ca^{2+} (157). Together with our work, these data suggest that even within a cell, myosin VI integrates protein, lipid, and Ca^{2+} cargo to perform its function in a site-specific manner.

Our findings therefore support a new model of myosin VI activation where, rather than having a given cargo for a given function, myosin VI integrates multiple signals on a given membrane in order to activate (**Figure 15**). Regulation through splicing biases myosin VI to certain protein cargo adaptors (15). The protein cargos regulate the localization of myosin VI in the cell, and may also be the primary determinant of myosin VI's oligomeric state (1). Once on-site, secondary cargo signals such as lipids or Ca^{2+} may fine-tune myosin VI's activity at that location by increasing myosin VI's effective affinity for its substrate, committing it to activate on that cargo (109).

LOVDab is a unique optogenetic tool in that it activates full-length myosin VI without altering the myosin itself, allowing for direct inferences on myosin VI activity and regulation *in vitro* and *in vivo*. LOVDab exhibits robust, light-dependent myosin VI recruitment to many different organelles, and myosin binding to LOVDab propels actin filaments in vitro. Using LOVDab, we discovered evidence for a new activation model for human myosin VI, whereby myosin VI integrates its activation signals to obtain a site-specific mode of activation. We believe that LOVDab will continue to be an extremely useful tool for answering questions about how this important motor protein functions in the cell.

3.5 Material & Methods

Protein purification

Full-length human myosin VI with an N-terminal FLAG-mCherry2B fusion was incorporated into baculovirus as discussed above. SF9 cells were infected at a 1:1 MOI and proteins were harvested from SF9 cells 58-72 hours post infection. The cells were re-suspended in Lysis buffer (see below for recipes) containing 2 mM ATP, and a cocktail of protease inhibitors including 1mM phenylmethylsulfonyl fluoride (PMSF) and 10μg/mL each of: aprotinin, leupeptin, chymostatin, and pepstatin A. The cells were lysed by douncing and nutated for 40 minutes at 4^{o}C to allow the myosin VI to diffuse out of the cells. The lysate was spun at 14,000 rpm in a Legend X1R centrifuge (F15S-8x50c rotor, Thermo Scientific) and a variable amount of anti-FLAG resin (M2, Sigma) added to the supernatant. After incubation, the resin was spun out of suspension at 900xg in a 5810R centrifuge (A-4-81 rotor, Eppendorf) and washed with wash buffer (see below) containing 3 mM ATP, a variable amount of Calmodulin, and protease inhibitors. Resin was repelleted using the same procedure and re-suspended in wash buffer

before transferred to a drip column where the resin was further washed. Resin was then incubated with elution buffer (wash buffer + 0.2 mg/mL FLAG peptide) for 1 hour. Protein was eluted and dialyzed against wash buffer containing no ATP or protease inhibitors. In the low salt preps (see text) the lysis buffer was 50 mM Tris·HCl, 150 mM KCl, 0.5 mM DTT, and 0.1% Triton X-100, pH = 7.7. The wash buffer was 20 mM imidazole, 150 mM KCl, 5 mM $MgCl_2$, 1 mM EDTA, and 1 mM EGTA, and 0.5 mM DTT, pH = 7.5. The storage/dialysis buffer was either AB: 25mM imidazole, 25 mM KCl, 4 mM Mg_2Cl_2, 1mM EGTA, 2mM DTT, pH = 7.5; or KMg25: 10 mM MOPS, 25 mM KCl, 1 mM EGTA, 1 mM $MgCl_2$, and 1 mM DTT, pH = 7.0. For the high salt prep, the lysis buffer was 50 mM Tris·HCl, 150 mM KCl, 0.5 mM EDTA, 1 mM EGTA, 4 mM $MgCl_2$, 0.5 mM DTT, and 0.1% Triton X-100, pH = 7.3, and the final dialysis/assay buffer was 50mM Tris·HCl, 150 mM KCl, 1 mM EDTA, 1mM EGTA, 5 mM MgCl2, and 0.5 mM DTT (1 mM DTT for final dialysis), pH = 7.3. For both preps, buffers were chilled to 0-4 $^{\circ}$C before use. pH values were set at room temperature.

Gliding filament assay

Nitrocellulose-coated coverslips were first coated in anti-GFP antibody (clone 3E6 MP Biomedicals, California, USA) at 0.25 μg/mL in PBS. Following this, coverslips were blocked using 1 mg/mL BSA (ELISA grade, EMD Millipore) and the antibody saturated using EGFP-LOV2Dab2^{pep} at 1 μM. After this, the slide was washed using KMg25 and a solution containing myosin VI, F-actin, and a radical scavenging system (0.45% glucose (w/v) 0.5% (v/v) BME, 432 μg/mL glucose oxidase, and 72 μg/mL catalase (158) was flowed in. Slides were then imaged using an x100, 1.65 NA objective (Olympus) on a custom-built total internal reflection microscope employing an EMCCD camera (iXon; Andor Technologies). This microscope was

controlled with the open source Micro-Manager program (www.micro-manager.org). For assays involving lipid cargo, artificial liposomes from Echelon Biosciences (Utah, USA) containing 5% of the signaling lipid $PI(4,5)P_2$ were added to the assay buffer. The liposomes had no effect on myosin VI activity if Ca^{2+} was not present at a total concentration of at least 1.5 mM (corresponding to a free Ca^{2+} concentration of approximately 25 μM). The necessity of Ca^{2+} matches previous results but this concentration is approximately tenfold lower than previously used for assessing the interaction of lipids with the myosin VI tail domain (136).

Gliding filament velocities were calculated from at least 3 videos from at least 2 independent preparations of myosin VI, using at least 10 filaments/video and at least 10 frames/filament. MTrackJ was used to generate the actin tracks (159). Filaments showing pausing were avoided in order to obtain an accurate estimate of "live" full length myosin VI activity. To quantify the length of actin on the coverslip, images were background subtracted and thresholded to create binary images of the actin that were then skeletonized using the ImageJ function. The sum of pixels in the images were converted to length using the pixel calibration and used as the estimate for the length of actin on the coverslip.

Chapter 4

Future directions and concluding remarks

4.1 Extending this work to studying myosin VI

Here I presented data showing that our designed tool LOVDab can reversibly recruit myosin VI using light. This design differs from previous optogenetic methods for manipulating motor protein control in that it does not require alteration of the myosin motor itself (142, 143, 160). Two groups have previously developed methods for recruiting constitutively active, truncated, forced-dimer motor proteins (142, 143). This method has the benefit of being able to recruit motors from any of the three superfamilies of motor proteins. However, while it is a facile method of force generation in vivo, this technique prevents the study of truly native motor behavior by eliminating the cargo binding domains, and there for native regulatory mechanisms, of these motors. The Bryant lab has inserted a LOV2 domain into the lever arm of myosin VI (160). Exciting the LOV2 domain in their LOV2-myosin VI fusion is sufficient to reverse the direction of the motor, conclusively demonstrating that the myosin VI lever arm is solely responsible for its reverse direction compared to other myosins. However, the stepping rate of their motors is less than 10 nm/sec, and its tail significantly altered, making this motor unsuitable for studying native myosin VI behavior (160). Our design improves over these approaches by simultaneously recruiting and activating myosin VI through its native cargo recruitment pathway, allowing us to study myosin VI with unprecedented precision.

After establishing that LOVDab can recruit and activate myosin VI, I used it to demonstrate that lipid and Ca^{2+} cargoes can influence myosin VI affinity of its protein cargo in a membrane specific manner inside the cell. As outlined in **Figure 6E** above, myosin VI regulation begins at transcription, where different splice forms of myosin VI are biased toward different classes of

protein cargo. Myosin VI can contain any combination of a long insert (LI) and short insert (SI) in its tail domains. Recent crystallographic evidence shows that the LI sterically occludes the RRL motif in the myosin tail that binds to the optineurin class of cargo proteins (15). Less is known regarding the structure of the region containing the SI, though phosphorylation of this insert is important for maintaining secretory granule localization in PC12 cells, an interaction that requires Ca^{2+} (96). LOVDab presents a unique and facile method for interrogating the roles each of these inserts has on the mechanical properties of myosin VI. It would be informative to the field to quantify the dependence of myosin VI motility on Ca^{2+} and lipids for each isoform using our modified gliding filament assay. Following this, mutational analysis could be used to determine whether the Ca^{2+}-driven enhancement always occurs through the calmodulin domains on the myosin lever arm. It could conceivably occur through another site that is dependent on the presence or absence of the splice inserts. For example, perhaps phosphorylation of the SI exposes a new calmodulin binding site on the distal tail that influences cargo interactions at that site.

Beyond Ca^{2+}, our study also implicates that myosin VI integrates lipid cargo in a Ca^{2+}-dependent manner. Thus, a further extension of this and other studies would be to quantify the lipid dependence of each isoform (136). Of particular interest is whether different isoforms prefer lipids that correspond to their membranes of choice *in vivo*. This finding would significantly underscore our results and the relevance of cargo integration by myosin VI.

A third level question is the structural mechanisms by which this integration takes place. In principle, this integration could simply be the result of increased avidity of a molecule with multiple binding partners on a single substrate. Either way, how myosin VI is able to bind directly to the membrane and to cargo proteins is difficult to envision without a structure of the complete tail domain. A complete structure of full length myosin VI in both the unbound and

cargo-saturated forms remains the ultimate goal of researchers wanting to understand myosin VI function. In addition to elucidating the impact of cargo on the CBD, understanding the interaction between the myosin VI head and its CBD is also of great interest, particularly in explaining why inhibition of its ATPase does not occur. The ideas presented here, that myosin VI integrates each of its cargoes, also may aid structural biologists in choosing better screening conditions for crystallography.

A final detail of myosin VI operation that needs to be addressed is whether myosin VI is in all cases active as a dimer *in vivo*. A study showing that dimeric Dab2 and optineurin cargos could dimerize myosin VI *in vitro* suggests that cargos can dimerize myosin VI for transport roles in the cell (1). However, since many of myosin VI's roles in the cell seem to be anchoring roles, which in theory would not require a processive dimer, these studies together suggest that the oligomeric state of myosin VI may be set by location-specific cargo *in vivo.* The oligomeric state of a myosin can be determined by calculating the power of the dependence of actin filament landing rate on myosin concentration in a gliding filament assay. One could directly assess the oligomeric state through crosslinking studies, such as with the zero length crosslinking 1-ethyl-3-(3-dimethylaminopropyl) carbodiimide (EDC) (136), or by fluorescence resonance energy transfer (FRET) (161). In the latter technique, fusing donor and acceptor FPs to the LOVDab C-terminus, rather than at the LOVDab N-terminus where the FPs were placed for this study, may be a viable approach to real-time detection of myosin VI dimerization in the cell using FRET. Thus, LOVDab presents a facile means of interrogating the cargo- and isoform-specific oligomeric states of myosin VI.

A natural extension of this study is to determine whether lipids and Ca^{2+} play any role in altering myosin VI's state in a given location in the cell. One could envision a pair of monomeric

myosin VI motors in an anchoring role being rapidly dimerized by these secondary messengers and converted into a transporter that could, for example, deliver a secretory vesicle to the plasma membrane.

Quantifying the Dab2^{pep}-myosin-lipid-Ca^{2+} interaction in vitro, will also functionally calibrate LOVDab to serve as a pseudo lipid/Ca2+ sensor in vivo. In effect, LOVDab could be used to map the cell for myosin VI binding aptitude, and to determine where in the cell the different myosin VI isoforms prefer to bind. Combining isoform mapping in the cell with cargo knockouts would make this approach exceptionally powerful for detecting myosin VI's small molecule binding partners, such as $PI(4,5)P_2$, in the cell.

The high temporal precision offered by LOVDab also makes it possible to assess off rate kinetics of myosin VI bindings in the cell. Using LOVDab together with additional fluorescence based small molecule sensors can further deconvolute the signals read in by myosin VI. For example, the ATP/ADP sensor PercevalHR could be used to assess whether myosin VI recruitment depends on the local metabolic state of an organelle, or whether this rate can influence whether myosin VI can act as an anchor or transporter (162). There are also a wide variety of fluorescent protein-based Ca^{2+} sensors available which can be used with LOVDab to directly test whether myosin VI recruitment correlates with Ca^{2+} transients in the cell (163). Fluorescent reporters for $PI(4,5)P_2$ could be used similarly for the lipid component of myosin VI activation (164).

4.2 Methods for improving the performance of LOVDab

I tested many obvious mutations when optimizing LOVDab, but it likely could still be improved. Qualitatively, the consistent limitation of LOVDab both *in vivo* and *in vitro* is its low affinity for

myosin VI relative to the low expression of this motor. Therefore, any attempt to improve on LOVDab should aim to increase the LOVDab - myosin VI affinity.

Dimerization with an N-terminal GCN4 leucine zipper did not seem to confer any advantage to LOVDab's performance. However, certain flanking residues can force GCN4 to adopt an antiparallel coiled-coil, which would extend the two Dab2^{pep}s in a GCN4-FP-LOVDab fusion protein out from each other. This antiparallel arrangement could therefore prevent dimerization by separating the Dab^{pep} cargoes too far from each other to bind across the CBDs of the same myosin VI dimer. Though I always used a short GGSEG linker between the GCN4 and the FP, it is possible that a longer linker here or elsewhere in the protein would better orient LOVDab for dimerizing myosin VI.

In terms of modifying the LOVDab sequence itself, I did not try a mutation series containing a phenylalanine residue in the L546 position in the Jα helix. The significance of this position is discussed in **Section 2.5** above. It is possible that by placing a phenylalanine at this position, and moving the Dab2^{pep} sequence further out from the Jα helix, that LOVDab would retain switching capabilities but gain a lit state affinity for myosin VI similar to LOVDab$_{+ctrl}$.

Beyond rational changes, mutational screens have seen success in optimizing other optogenetic tools (55). In LOVDab, the mutational search could target either LOV2 or Dab2pep. Mutating Dab2pep to directly bind myosin VI more tightly is appealing since it should merely shift the dynamic range of LOVDab without altering the switching behavior of the protein itself. However, the fast off rate of myosin VI from LOVDab is beneficial to its high temporal control of myosin VI, and mutations on the Dab2^{pep} may reduce this. Additionally, mutations to Dab2^{pep} may alter the ways in which myosin VI integrates protein cargo with other activation signals.

Mutating Dab2^{pep} could therefore remove the ability to use LOVDab to interrogate myosin VI behavior, limiting its usefulness.

Screening for mutations that improve LOVDab switching that are within the LOV2 domain is appealing in that it maintains the native interaction of Dab2pep with myosin VI and can conceivably result in a myosin activator with a larger dynamic range than the current design. However, LOV2 has much more sequence space than Dab2^{pep}, which means consideration must be put into the design of the screen to adequately explore this space. Furthermore, the complexity of the LOV2 conformational change makes interpretations of the effects of LOV2 mutations more difficult than for Dab2^{pep} (57, 67). While it is up to the experimenter, my opinion is that preserving the native interaction between Dab2^{pep} and myosin VI outweighs these other concerns.

Perhaps the most sensible way to extend the impact of LOVDab is to fuse LOV2 to other peptides that bind and activate myosin VI, or even other myosins. As reviewed in **Section 1.3.1 above**, Ca^{2+} and lipid binding play a role in regulating many different myosins in the cell. The exact relevance of Ca^{2+} is still unclear for many motors such as myosin Va, where its ability to promote myosin motility while releasing calmodulin from the IQ domains appears to oppose itself (75, 92). One reason for this discrepancy could be that Ca^{2+} modulates myosin:protein cargo interactions in the cell, and that studies measuring the effects of either cargo on myosin independently do not sufficiently recreate the *in vivo* environment of myosin VI. Extending the methodology behind LOVDab will allow us to determine whether cargo signal integration is indeed a generalizable property of myosins, or motor proteins in general. Controlling multiple motors through their native cargo will also allow researchers to reassemble multi-myosin systems and study their interaction in a much more realistic setting.

4.3 Concluding remarks

At the turn of the 20th century single molecule studies of truncated, forced-dimer motor proteins greatly expanded the field of motor protein research. These studies removed the native regulatory domains of myosins in order to study the intrinsic, biophysical mechanisms of force-generation by motor domains in isolation. But it is increasingly clear that, if we are to understand the function of this important class of proteins within living organisms, we cannot do so apart from their regulatory tail domains or the various cargo signals that they bind. This is especially apparent for myosin VI, whose regulatory domains may play a direct role in determining what type of function the motor head plays at a given time and location inside the cell. To this end, I have successfully engineered an optogenetic method for controlling and studying myosin VI with high spatial and temporal resolution. This approach may theoretically be extended to controlling other auto-inhibited motor proteins through their cargo binding domains. I believe tools like these will greatly enhance humankind's understanding of motor protein function.

Appendix A1

The LOV2 β-bulge

Among the conserved residues in the *Avena sativa* LOV2 (AsLOV2) domain, we identified an unusual three-residue β-bulge that is conserved across all PAS domains with known structures and comes from all kingdoms of life (33). The billion-year conservation of this motif located at the amino terminus of the Bβ-strand (I427-I428-F429 in AsLOV2) sharply contrasts with the extensive diversity in PAS function and the type and location of ligands within PAS domains. Suspecting that this region would be functionally sensitive, I extensively mutated it. I found only moderate effects, except for a charged I428D substitution that expressed poorly. We tentatively conclude that the highly conserved bulge structure is a legacy that is difficult to evolve away without compromising foldability. This underscores the finding by Zayner *et al* that conservation is not an accurate predictor of function in AsLOV2 (67).

Appendix A2

LOLOVV: a LOV2 within a LOV2 domain

One region in the LOV2 domain that has not been extensively mutated is the LOV2-Jα loop, which consists of residues 517-520 (57, 67). This region is attractive as it may be mutated to extend the reach of the Jα helix in its unfolded state with minimal perturbation of the LOV2:Jα interaction in the dark state. To this end, I sought to improve the switching capability of the LOV2 domain by replacing this loop with another LOV2 domain to create LOLOVV. My goal was to fuse the two proteins in such a way as to fully preserve the degree of light-driven conformational change in both domains, or to enhance it by creating a single, continuous helix consisting of the Jα helices of both LOV2 domains.

A I427V mutation, which greatly increases the photorecovery rate of the LOV2 domain (165), was included on the inner LOLOVV (**Figure A2A**) in order to detect the photocycles of each individual LOV2 domain. Comparison of the UV/Vis absorption spectra for LOLOVV indicates that LOLOVV bleaches fully in the light, showing it is fully photoresponsive (**Figure A2B**). Inserting a C450V mutation, which prevents the photocycle from occurring, into either the inner or outer LOV2 domain limits the bleaching to about 50% of normal values. Together these suggest both LOV2 domains in LOLOVV completely photocycle. **Figure A2C** shows that the CD change for the LOLOVV domain matches the combined CD change for its constituent LOV2 domains, both in rate and magnitude. Note that the δCD for LOLOVVs containing a C450V mutation are about half the wildtype value of 0.3 (57), since there are twice the LOV2 domains present per molecule. As a note of caution, this data was not buffer subtracted. For typical values of buffer at 222 nm in our system, the δCD for LOLOVV could range from 0.25-0.3, very close to that for wildtype LOV2.

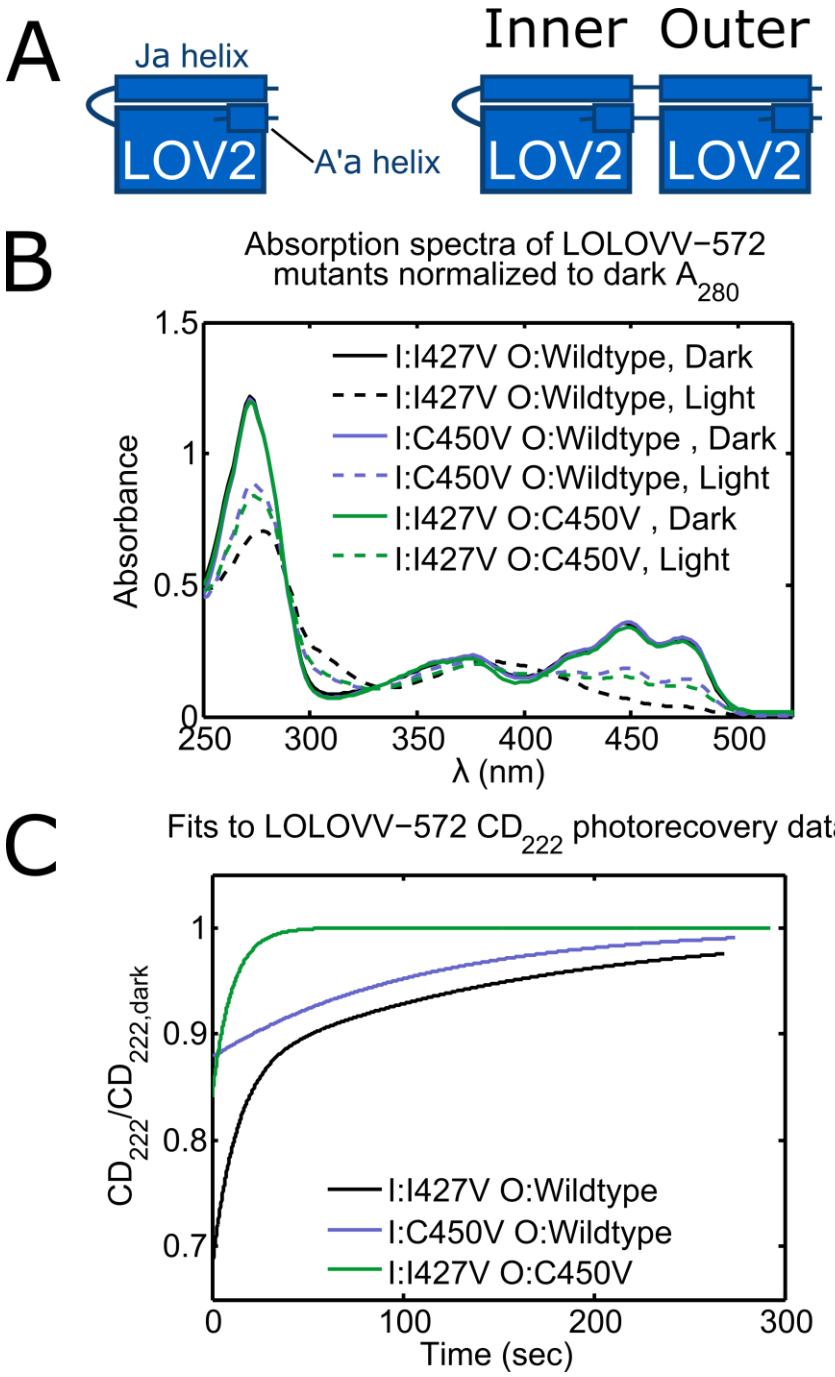

Figure A2. LOLOVV maintains photocycle in both its constituent LOV2 domains. (**A**) LOLOVV design. *Left*: cartoon depiction of the LOV2 domain with its terminal Jα and A'α helices labeled. *Right*: LOLOVV is made of a LOV2 domain inserted into the Jα-LOV2 loop of another LOV2 domain. (**B**) UV/Vis spectra of LOLOVV constructs, normalized to their A280 value in the dark. LOLOVV fully bleaches but a C450V mutation in either LOV2 domain limits bleaching to 50% the level in the dark, indicating both LOV2 domains are active. I: inner. O: outer. (**C**) Fits to the CD photorecovery at 222 nm show that the conformational change in LOLOVV is roughly the sum of its constituent LOV2 domains, both in rate and magnitude.

The above data are presented for LOLOVV 572. However, LOLOVV constructs expressed well and were fairly tolerable to mutations at the linker regions on either side, provided they were of sufficient length (**Table A2**). These linkers each utilize engineered restriction sites in the LOV2 domain, including a silent *EagI* site on the 3' end of the LOV2-Jα loop and a *SalI* site on the 5' end that causes a conservative T517V/E518D double mutation. I have named the LOV2 domain containing these inserts RELOV, for "Restriction Endonuclease LOV2." RELOV also contains a silent *SacI* site at E545 to ease C-terminal ligations to LOV2. Mutations desired in the outer LOV2 domain, including any N- or C-terminal fusion proteins, are quikchanged/ligated into the RELOV plasmid. Mutations desired on the inner LOV2 are made on a LOV2 gene not containing the RELOV mutations. The inner LOV2 domain is amplified using PCR and then ligated into digested RELOV plasmid. The overhanging regions on the primers used for amplifying the inner LOV2 gene must contain the SalI and EagI sites, and the desired linker region. This process is important since LOLOVV contains two copies of the LOV2 domain, making direct quikchange within the LOLOVV domain impossible.

Table A2: LOLOVV constructs and their linker sequences

Name	LOV2-N' linker-LOV2	LOV2-C' linker-LOV2	Expression
LOLOVV	VD--LAT	KEL-S-VRDAA	N.D.
-412	VD--LAT	KEL-S-RDAA	+
-413	VD--LAT	KEL--VRDAA	+
-57	VD-GSG-GEFLAT	KEL-GSG-VRDAA	++
-572	VD-GSG-GEFLAT	K-AAA-RDAA	++
-2.1	VD--LAT	KEL--AA	N.D.
-2.2	VD--LAT	K-AAK-AA	N.D.
-2.3	VD--LAT	K-AA-DAA	++
-2.4	VD--GEFLAT	K-AAK-AA	+
-2.5	VD--FLAT	K-AAK-AA	++
-2.6	VD-GID-FLAT	K-AAK-AA	++

Appendix A3

Light-dependent actin binding

LifeAct is a 17 residue N-terminal peptide fragment from the *Saccharomyces cerevisiae* Abp140 protein (166). Its amino acid sequence is MGVADLIKKFESISKEE. Blocking LifeAct with LOV2 in a light-dependent manner could create a tool for inducible recruitment to the actin cytoskeleton, which could have several applications for biologists. I made a series of mCherry-LOV2-LifeAct (MLLA) fusion proteins and sought to screen them using an actin cosedimentation assay. In this assay, actin filaments are incubated with a protein of interest, and subsequently pelleted in an ultracentrifuge. The actin brings the proteins it has bound into the pellet. The supernatant containing unbound protein is removed, and the pellet is resolubilized. The amount of unbound protein and bound protein are then quantified by running the supernatant and resolubilized pellet samples on an SDS-PAGE gel, respectively. From this information, a binding constant can be calculated.

Since the actin must be pelleted in the dark, in order to look for light-dark differences in MLLA constructs I made the "lit-state control" I539E mutation to constitutively unfold the Jα helix in the dark (70). Plotting the fraction bound MLLA as a function of concentration, it is clear that none of my constructs have a significant light-dark difference in binding to actin (**Figure A3**).

Unfortunately, the cosedimentation assay was noisy, and I did not have a protein that could serve as a positive control for myosin VI binding. LifeAct is in fast equilibrium with actin in vivo (166), so extra care is needed to pellet the actin and remove the supernatant quickly without disturbing the pellet. Additionally, at the time I was doing experiments little information was

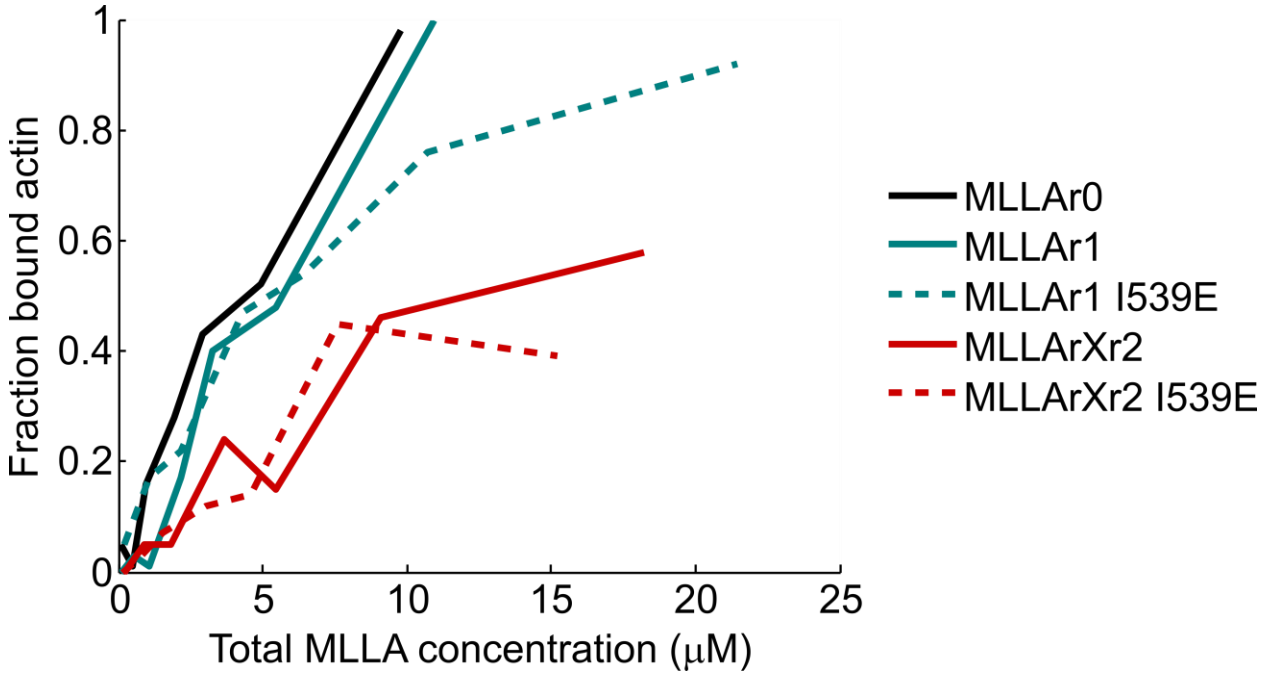

Figure A3. MLLA actin binding assessed with the actin cosedimentation assay. Each mutant contains the T406A/T407A double mutation. Neither the r1 nor rXr2 variant shows significant light-dependent caging of LifeAct. For sequence information, see **Table A3**.

known on the key actin binding residues in the LifeAct peptide. Thus, I could not make rational mutations to block these residues, but did a series of simple truncations (**Table A3**). Nonetheless, the cosedimentation assay is simple to learn and can directly detect binding. I recommend that if this project is taken up again that one first performs alanine scanning mutagenesis or a similar mutagenesis strategy to first identify the key actin binding residues on LifeAct, if this has not been published in the literature. This will greatly reduce the size of mutational space needed to search for the rational design of a LOV2-LifeAct fusion protein that shows light-dependent binding.

Table A3: MLLA construct sequences

Name	Fusion sequence …LOV2-LifeAct…	Mutations
MLLAr0	…AKEL-MGV…	406A/407A
-r1	…AK-MGV…	406A/407A
-r2	…AA-MGV…	406A/407A
-r1r2	…AK-V…	406A/407A
-r2r2	…A-V…	406A/407A
-rXr2	…AKE-V…	406A/407A
-r1 G2A	…AK-MAV…	406A/407A/G2A

References cited

1. Phichith D, Travaglia M, Yang Z, Liu X, Zong AB, Safer D, et al. Cargo binding induces dimerization of myosin VI. Proc Natl Acad Sci U S A. 2009;106(41):17320-4.

2. Kachaner D, Genin P, Laplantine E, Weil R. Toward an integrative view of Optineurin functions. Cell Cycle. 2012;11(15):2808-18.

3. Laplantine E, Fontan E, Chiaravalli J, Lopez T, Lakisic G, Veron M, et al. NEMO specifically recognizes K63-linked poly-ubiquitin chains through a new bipartite ubiquitin-binding domain. EMBO J. 2009;28(19):2885-95.

4. Gautier A, Gauron C, Volovitch M, Bensimon D, Jullien L, Vriz S. How to control proteins with light in living systems. Nat Chem Biol. 2014;10(7):533-41.

5. Fenno L, Yizhar O, Deisseroth K. The development and application of optogenetics. Annu Rev Neurosci. 2011;34:389-412.

6. Tischer D, Weiner OD. Illuminating cell signalling with optogenetic tools. Nat Rev Mol Cell Biol. 2014;15(8):551-8.

7. Wells AL, Lin AW, Chen LQ, Safer D, Cain SM, Hasson T, et al. Myosin VI is an actin-based motor that moves backwards. Nature. 1999;401(6752):505-8.

8. Rock RS, Rice SE, Wells AL, Purcell TJ, Spudich JA, Sweeney HL. Myosin VI is a processive motor with a large step size. Proc Natl Acad Sci U S A. 2001;98(24):13655-9.

9. Buss F, Arden SD, Lindsay M, Luzio JP, Kendrick-Jones J. Myosin VI isoform localized to clathrin-coated vesicles with a role in clathrin-mediated endocytosis. EMBO J. 2001;20(14):3676-84.

10. Self T, Sobe T, Copeland NG, Jenkins NA, Avraham KB, Steel KP. Role of myosin VI in the differentiation of cochlear hair cells. Dev Biol. 1999;214(2):331-41.

11. Warner CL, Stewart A, Luzio JP, Steel KP, Libby RT, Kendrick-Jones J, et al. Loss of myosin VI reduces secretion and the size of the Golgi in fibroblasts from Snell's waltzer mice. EMBO J. 2003;22(3):569-79.

12. Tumbarello DA, Waxse BJ, Arden SD, Bright NA, Kendrick-Jones J, Buss F. Autophagy receptors link myosin VI to autophagosomes to mediate Tom1-dependent autophagosome maturation and fusion with the lysosome. Nat Cell Biol. 2012;14(10):1024-35.

13. Sahlender DA, Roberts RC, Arden SD, Spudich G, Taylor MJ, Luzio JP, et al. Optineurin links myosin VI to the Golgi complex and is involved in Golgi organization and exocytosis. J Cell Biol. 2005;169(2):285-95.

14. He F, Wollscheid HP, Nowicka U, Biancospino M, Valentini E, Ehlinger A, et al. Myosin VI Contains a Compact Structural Motif that Binds to Ubiquitin Chains. Cell Rep. 2016;14(11):2683-94.

15. Wollscheid HP, Biancospino M, He F, Magistrati E, Molteni E, Lupia M, et al. Diverse functions of myosin VI elucidated by an isoform-specific alpha-helix domain. Nat Struct Mol Biol. 2016;23(4):300-8.

16. Bugaj LJ, Choksi AT, Mesuda CK, Kane RS, Schaffer DV. Optogenetic protein clustering and signaling activation in mammalian cells. Nat Methods. 2013;10(3):249-52.

17. Toettcher JE, Gong D, Lim WA, Weiner OD. Light-based feedback for controlling intracellular signaling dynamics. Nat Methods. 2011;8(10):837-9.

18. Levskaya A, Weiner OD, Lim WA, Voigt CA. Spatiotemporal control of cell signalling using a light-switchable protein interaction. Nature. 2009;461(7266):997-1001.

19. Kumar A, Ali AM, Woolley GA. Photo-control of DNA binding by an engrailed homeodomain-photoactive yellow protein hybrid. Photochem Photobiol Sci. 2015;14(9):1729-36.

20. Strickland D, Yao X, Gawlak G, Rosen MK, Gardner KH, Sosnick TR. Rationally improving LOV domain-based photoswitches. Nat Methods. 2010;7(8):623-6.

21. Strickland D, Lin Y, Wagner E, Hope CM, Zayner J, Antoniou C, et al. TULIPs: tunable, light-controlled interacting protein tags for cell biology. Nat Methods. 2012;9(4):379-84.

22. Wu YI, Frey D, Lungu OI, Jaehrig A, Schlichting I, Kuhlman B, et al. A genetically encoded photoactivatable Rac controls the motility of living cells. Nature. 2009;461(7260):104-8.

23. Chaves I, Pokorny R, Byrdin M, Hoang N, Ritz T, Brettel K, et al. The cryptochromes: blue light photoreceptors in plants and animals. Annu Rev Plant Biol. 2011;62:335-64.

24. Hoang N, Bouly JP, Ahmad M. Evidence of a light-sensing role for folate in Arabidopsis cryptochrome blue-light receptors. Mol Plant. 2008;1(1):68-74.

25. Christie JM, Blackwood L, Petersen J, Sullivan S. Plant flavoprotein photoreceptors. Plant Cell Physiol. 2015;56(3):401-13.

26. Cailliez F, Muller P, Gallois M, de la Lande A. ATP binding and aspartate protonation enhance photoinduced electron transfer in plant cryptochrome. J Am Chem Soc. 2014;136(37):12974-86.

27. Muller P, Bouly JP. Searching for the mechanism of signalling by plant photoreceptor cryptochrome. FEBS Lett. 2015;589(2):189-92.

28. Mas P, Devlin PF, Panda S, Kay SA. Functional interaction of phytochrome B and cryptochrome 2. Nature. 2000;408(6809):207-11.

29. Kennedy MJ, Hughes RM, Peteya LA, Schwartz JW, Ehlers MD, Tucker CL. Rapid blue-light-mediated induction of protein interactions in living cells. Nat Methods. 2010;7(12):973-5.

30. Liu H, Yu X, Li K, Klejnot J, Yang H, Lisiero D, et al. Photoexcited CRY2 interacts with CIB1 to regulate transcription and floral initiation in Arabidopsis. Science. 2008;322(5907):1535-9.

31. Bugaj LJ, Spelke DP, Mesuda CK, Varedi M, Kane RS, Schaffer DV. Regulation of endogenous transmembrane receptors through optogenetic Cry2 clustering. Nat Commun. 2015;6:6898.

32. Nagy A. Cre recombinase: the universal reagent for genome tailoring. Genesis. 2000;26(2):99-109.

33. Moglich A, Ayers RA, Moffat K. Structure and signaling mechanism of Per-ARNT-Sim domains. Structure. 2009;17(10):1282-94.

34. Hefti MH, Francoijs KJ, de Vries SC, Dixon R, Vervoort J. The PAS fold. A redefinition of the PAS domain based upon structural prediction. Eur J Biochem. 2004;271(6):1198-208.

35. Halavaty AS, Moffat K. N- and C-terminal flanking regions modulate light-induced signal transduction in the LOV2 domain of the blue light sensor phototropin 1 from Avena sativa. Biochemistry. 2007;46(49):14001-9.

36. Christie JM, Salomon M, Nozue K, Wada M, Briggs WR. LOV (light, oxygen, or voltage) domains of the blue-light photoreceptor phototropin (nph1): binding sites for the chromophore flavin mononucleotide. Proc Natl Acad Sci U S A. 1999;96(15):8779-83.

37. Sevvana M, Vijayan V, Zweckstetter M, Reinelt S, Madden DR, Herbst-Irmer R, et al. A ligand-induced switch in the periplasmic domain of sensor histidine kinase CitA. J Mol Biol. 2008;377(2):512-23.

38. Zoltowski BD, Schwerdtfeger C, Widom J, Loros JJ, Bilwes AM, Dunlap JC, et al. Conformational switching in the fungal light sensor Vivid. Science. 2007;316(5827):1054-7.

39. Matsuoka D, Tokutomi S. Blue light-regulated molecular switch of Ser/Thr kinase in phototropin. Proc Natl Acad Sci U S A. 2005;102(37):13337-42.

40. Lungu OI, Hallett RA, Choi EJ, Aiken MJ, Hahn KM, Kuhlman B. Designing photoswitchable peptides using the AsLOV2 domain. Chem Biol. 2012;19(4):507-17.

41. Strickland D, Moffat K, Sosnick TR. Light-activated DNA binding in a designed allosteric protein. Proc Natl Acad Sci U S A. 2008;105(31):10709-14.

42. Moglich A, Ayers RA, Moffat K. Design and signaling mechanism of light-regulated histidine kinases. J Mol Biol. 2009;385(5):1433-44.

43. Rockwell NC, Su YS, Lagarias JC. Phytochrome structure and signaling mechanisms. Annu Rev Plant Biol. 2006;57:837-58.

44. Quail PH. Phytochrome photosensory signalling networks. Nat Rev Mol Cell Biol. 2002;3(2):85-93.

45. Butler WL, Norris KH, Siegelman HW, Hendricks SB. Detection, Assay, and Preliminary Purification of the Pigment Controlling Photoresponsive Development of Plants. Proc Natl Acad Sci U S A. 1959;45(12):1703-8.

46. Takala H, Bjorling A, Berntsson O, Lehtivuori H, Niebling S, Hoernke M, et al. Signal amplification and transduction in phytochrome photosensors. Nature. 2014;509(7499):245-8.

47. Ni M, Tepperman JM, Quail PH. Binding of phytochrome B to its nuclear signalling partner PIF3 is reversibly induced by light. Nature. 1999;400(6746):781-4.

48. Meyer TE. Isolation and characterization of soluble cytochromes, ferredoxins and other chromophoric proteins from the halophilic phototrophic bacterium Ectothiorhodospira halophila. Biochim Biophys Acta. 1985;806(1):175-83.

49. Meyer TE, Yakali E, Cusanovich MA, Tollin G. Properties of a water-soluble, yellow protein isolated from a halophilic phototrophic bacterium that has photochemical activity analogous to sensory rhodopsin. Biochemistry. 1987;26(2):418-23.

50. Sprenger WW, Hoff WD, Armitage JP, Hellingwerf KJ. The eubacterium Ectothiorhodospira halophila is negatively phototactic, with a wavelength dependence that fits the absorption spectrum of the photoactive yellow protein. J Bacteriol. 1993;175(10):3096-104.

51. Briggs WR, Christie JM. Phototropins 1 and 2: versatile plant blue-light receptors. Trends Plant Sci. 2002;7(5):204-10.

52. Morgan SA, Woolley GA. A photoswitchable DNA-binding protein based on a truncated GCN4-photoactive yellow protein chimera. Photochem Photobiol Sci. 2010;9(10):1320-6.

53. Ali AM, Reis JM, Xia Y, Rashid AJ, Mercaldo V, Walters BJ, et al. Optogenetic Inhibitor of the Transcription Factor CREB. Chem Biol. 2015;22(11):1531-9.

54. Pudasaini A, El-Arab KK, Zoltowski BD. LOV-based optogenetic devices: light-driven modules to impart photoregulated control of cellular signaling. Front Mol Biosci. 2015;2:18.

55. Guntas G, Hallett RA, Zimmerman SP, Williams T, Yumerefendi H, Bear JE, et al. Engineering an improved light-induced dimer (iLID) for controlling the localization and activity of signaling proteins. Proc Natl Acad Sci U S A. 2015;112(1):112-7.

56. Harper SM, Neil LC, Gardner KH. Structural basis of a phototropin light switch. Science. 2003;301(5639):1541-4.

57. Zayner JP, Antoniou C, Sosnick TR. The amino-terminal helix modulates light-activated conformational changes in AsLOV2. J Mol Biol. 2012;419(1-2):61-74.

58. Crosson S, Moffat K. Structure of a flavin-binding plant photoreceptor domain: insights into light-mediated signal transduction. Proc Natl Acad Sci U S A. 2001;98(6):2995-3000.

59. Salomon M, Eisenreich W, Durr H, Schleicher E, Knieb E, Massey V, et al. An optomechanical transducer in the blue light receptor phototropin from Avena sativa. Proc Natl Acad Sci U S A. 2001;98(22):12357-61.

60. Swartz TE, Corchnoy SB, Christie JM, Lewis JW, Szundi I, Briggs WR, et al. The photocycle of a flavin-binding domain of the blue light photoreceptor phototropin. J Biol Chem. 2001;276(39):36493-500.

61. Nozaki D, Iwata T, Ishikawa T, Todo T, Tokutomi S, Kandori H. Role of Gln1029 in the photoactivation processes of the LOV2 domain in adiantum phytochrome3. Biochemistry. 2004;43(26):8373-9.

62. Nash AI, Ko WH, Harper SM, Gardner KH. A conserved glutamine plays a central role in LOV domain signal transmission and its duration. Biochemistry. 2008;47(52):13842-9.

63. Konold PE, Mathes T, Weibetaenborn J, Groot ML, Hegemann P, Kennis JT. Unfolding of the C-Terminal Jalpha Helix in the LOV2 Photoreceptor Domain Observed by Time-Resolved Vibrational Spectroscopy. J Phys Chem Lett. 2016;7(17):3472-6.

64. Freddolino PL, Gardner KH, Schulten K. Signaling mechanisms of LOV domains: new insights from molecular dynamics studies. Photochem Photobiol Sci. 2013;12(7):1158-70.

65. Zayner JP, Sosnick TR. Factors that control the chemistry of the LOV domain photocycle. PLoS One. 2014;9(1):e87074.

66. Conrad KS, Manahan CC, Crane BR. Photochemistry of flavoprotein light sensors. Nat Chem Biol. 2014;10(10):801-9.

67. Zayner JP, Antoniou C, French AR, Hause RJ, Jr., Sosnick TR. Investigating models of protein function and allostery with a widespread mutational analysis of a light-activated protein. Biophys J. 2013;105(4):1027-36.

68. Yumerefendi H, Lerner AM, Zimmerman SP, Hahn K, Bear JE, Strahl BD, et al. Light-induced nuclear export reveals rapid dynamics of epigenetic modifications. Nat Chem Biol. 2016;12(6):399-401.

69. Yao X, Rosen MK, Gardner KH. Estimation of the available free energy in a LOV2-J alpha photoswitch. Nat Chem Biol. 2008;4(8):491-7.

70. Harper SM, Christie JM, Gardner KH. Disruption of the LOV-Jalpha helix interaction activates phototropin kinase activity. Biochemistry. 2004;43(51):16184-92.

71. Spiltoir JI, Strickland D, Glotzer M, Tucker CL. Optical Control of Peroxisomal Trafficking. ACS Synth Biol. 2015.

72. Hartman MA, Spudich JA. The myosin superfamily at a glance. J Cell Sci. 2012;125(Pt 7):1627-32.

73. Buss F, Kendrick-Jones J. Multifunctional myosin VI has a multitude of cargoes. Proc Natl Acad Sci U S A. 2011;108(15):5927-8.

74. Odronitz F, Kollmar M. Drawing the tree of eukaryotic life based on the analysis of 2,269 manually annotated myosins from 328 species. Genome Biol. 2007;8(9):R196.

75. Heissler SM, Sellers JR. Various Themes of Myosin Regulation. J Mol Biol. 2016;428(9 Pt B):1927-46.

76. Buss F, Kendrick-Jones J. How are the cellular functions of myosin VI regulated within the cell? Biochem Biophys Res Commun. 2008;369(1):165-75.

77. De La Cruz EM, Wells AL, Rosenfeld SS, Ostap EM, Sweeney HL. The kinetic mechanism of myosin V. Proc Natl Acad Sci U S A. 1999;96(24):13726-31.

78. Muretta JM, Rohde JA, Johnsrud DO, Cornea S, Thomas DD. Direct real-time detection of the structural and biochemical events in the myosin power stroke. Proc Natl Acad Sci U S A. 2015;112(46):14272-7.

79. De La Cruz EM, Ostap EM. Relating biochemistry and function in the myosin superfamily. Curr Opin Cell Biol. 2004;16(1):61-7.

80. Cao L, Wang W, Jiang Q, Wang C, Knossow M, Gigant B. The structure of apo-kinesin bound to tubulin links the nucleotide cycle to movement. Nat Commun. 2014;5:5364.

81. Cross RA. Review: Mechanochemistry of the kinesin-1 ATPase. Biopolymers. 2016;105(8):476-82.

82. Roberts AJ, Kon T, Knight PJ, Sutoh K, Burgess SA. Functions and mechanics of dynein motor proteins. Nat Rev Mol Cell Biol. 2013;14(11):713-26.

83. Hancock WO. The Kinesin-1 Chemomechanical Cycle: Stepping Toward a Consensus. Biophys J. 2016;110(6):1216-25.

84. Bhabha G, Johnson GT, Schroeder CM, Vale RD. How Dynein Moves Along Microtubules. Trends Biochem Sci. 2016;41(1):94-105.

85. Sweeney HL, Houdusse A. Myosin VI rewrites the rules for myosin motors. Cell. 2010;141(4):573-82.

86. De La Cruz EM, Ostap EM, Sweeney HL. Kinetic mechanism and regulation of myosin VI. J Biol Chem. 2001;276(34):32373-81.

87. Hasson T, Mooseker MS. Porcine myosin-VI: characterization of a new mammalian unconventional myosin. J Cell Biol. 1994;127(2):425-40.

88. Menetrey J, Bahloul A, Wells AL, Yengo CM, Morris CA, Sweeney HL, et al. The structure of the myosin VI motor reveals the mechanism of directionality reversal. Nature. 2005;435(7043):779-85.

89. Sweeney HL, Park H, Zong AB, Yang Z, Selvin PR, Rosenfeld SS. How myosin VI coordinates its heads during processive movement. EMBO J. 2007;26(11):2682-92.

90. Krendel M, Mooseker MS. Myosins: tails (and heads) of functional diversity. Physiology (Bethesda). 2005;20:239-51.

91. Berg JS, Powell BC, Cheney RE. A millennial myosin census. Mol Biol Cell. 2001;12(4):780-94.

92. Hammer JA, 3rd, Sellers JR. Walking to work: roles for class V myosins as cargo transporters. Nat Rev Mol Cell Biol. 2012;13(1):13-26.

93. Sladewski TE, Krementsova EB, Trybus KM. Myosin Vc Is Specialized for Transport on a Secretory Superhighway. Curr Biol. 2016;26(16):2202-7.

94. Dance AL, Miller M, Seragaki S, Aryal P, White B, Aschenbrenner L, et al. Regulation of myosin-VI targeting to endocytic compartments. Traffic. 2004;5(10):798-813.

95. Au JS, Puri C, Ihrke G, Kendrick-Jones J, Buss F. Myosin VI is required for sorting of AP-1B-dependent cargo to the basolateral domain in polarized MDCK cells. J Cell Biol. 2007;177(1):103-14.

96. Tomatis VM, Papadopulos A, Malintan NT, Martin S, Wallis T, Gormal RS, et al. Myosin VI small insert isoform maintains exocytosis by tethering secretory granules to the cortical actin. J Cell Biol. 2013;200(3):301-20.

97. Heissler SM, Manstein DJ. Nonmuscle myosin-2: mix and match. Cell Mol Life Sci. 2013;70(1):1-21.

98. Bement WM, Mooseker MS. TEDS rule: a molecular rationale for differential regulation of myosins by phosphorylation of the heavy chain head. Cell Motil Cytoskeleton. 1995;31(2):87-92.

99. Buss F, Kendrick-Jones J, Lionne C, Knight AE, Cote GP, Paul Luzio J. The localization of myosin VI at the golgi complex and leading edge of fibroblasts and its phosphorylation and recruitment into membrane ruffles of A431 cells after growth factor stimulation. J Cell Biol. 1998;143(6):1535-45.

100. Naccache SN, Hasson T. Myosin VI altered at threonine 406 stabilizes actin filaments in vivo. Cell Motil Cytoskeleton. 2006;63(10):633-45.

101. Liu J, Taylor DW, Krementsova EB, Trybus KM, Taylor KA. Three-dimensional structure of the myosin V inhibited state by cryoelectron tomography. Nature. 2006;442(7099):208-11.

102. Thirumurugan K, Sakamoto T, Hammer JA, 3rd, Sellers JR, Knight PJ. The cargo-binding domain regulates structure and activity of myosin 5. Nature. 2006;442(7099):212-5.

103. Yang Y, Baboolal TG, Siththanandan V, Chen M, Walker ML, Knight PJ, et al. A FERM domain autoregulates Drosophila myosin 7a activity. Proc Natl Acad Sci U S A. 2009;106(11):4189-94.

104. Umeki N, Jung HS, Watanabe S, Sakai T, Li XD, Ikebe R, et al. The tail binds to the head-neck domain, inhibiting ATPase activity of myosin VIIA. Proc Natl Acad Sci U S A. 2009;106(21):8483-8.

105. Mukherjea M, Llinas P, Kim H, Travaglia M, Safer D, Menetrey J, et al. Myosin VI dimerization triggers an unfolding of a three-helix bundle in order to extend its reach. Mol Cell. 2009;35(3):305-15.

106. Park H, Ramamurthy B, Travaglia M, Safer D, Chen LQ, Franzini-Armstrong C, et al. Full-length myosin VI dimerizes and moves processively along actin filaments upon monomer clustering. Mol Cell. 2006;21(3):331-6.

107. Spink BJ, Sivaramakrishnan S, Lipfert J, Doniach S, Spudich JA. Long single alpha-helical tail domains bridge the gap between structure and function of myosin VI. Nat Struct Mol Biol. 2008;15(6):591-7.

108. McConnell RE, Tyska MJ. Leveraging the membrane - cytoskeleton interface with myosin-1. Trends Cell Biol. 2010;20(7):418-26.

109. Batters C, Brack D, Ellrich H, Averbeck B, Veigel C. Calcium can mobilize and activate myosin-VI. Proc Natl Acad Sci U S A. 2016;113(9):E1162-9.

110. Trybus KM, Gushchin MI, Lui H, Hazelwood L, Krementsova EB, Volkmann N, et al. Effect of calcium on calmodulin bound to the IQ motifs of myosin V. J Biol Chem. 2007;282(32):23316-25.

111. Gordon AM, Homsher E, Regnier M. Regulation of contraction in striated muscle. Physiol Rev. 2000;80(2):853-924.

112. Kudryashov DS, Reisler E. ATP and ADP actin states. Biopolymers. 2013;99(4):245-56.

113. Orlova A, Egelman EH. A conformational change in the actin subunit can change the flexibility of the actin filament. J Mol Biol. 1993;232(2):334-41.

114. Zimmermann D, Santos A, Kovar DR, Rock RS. Actin age orchestrates myosin-5 and myosin-6 run lengths. Curr Biol. 2015;25(15):2057-62.

115. Nagy S, Ricca BL, Norstrom MF, Courson DS, Brawley CM, Smithback PA, et al. A myosin motor that selects bundled actin for motility. Proc Natl Acad Sci U S A. 2008;105(28):9616-20.

116. Nagy S, Rock RS. Structured post-IQ domain governs selectivity of myosin X for fascin-actin bundles. J Biol Chem. 2010;285(34):26608-17.

117. Vavra KC, Xia Y, Rock RS. Competition between Coiled-Coil Structures and the Impact on Myosin-10 Bundle Selection. Biophys J. 2016;110(11):2517-27.

118. Park H, Li A, Chen LQ, Houdusse A, Selvin PR, Sweeney HL. The unique insert at the end of the myosin VI motor is the sole determinant of directionality. Proc Natl Acad Sci U S A. 2007;104(3):778-83.

119. Bryant Z, Altman D, Spudich JA. The power stroke of myosin VI and the basis of reverse directionality. Proc Natl Acad Sci U S A. 2007;104(3):772-7.

120. Menetrey J, Llinas P, Mukherjea M, Sweeney HL, Houdusse A. The structural basis for the large powerstroke of myosin VI. Cell. 2007;131(2):300-8.

121. Rock RS, Ramamurthy B, Dunn AR, Beccafico S, Rami BR, Morris C, et al. A flexible domain is essential for the large step size and processivity of myosin VI. Mol Cell. 2005;17(4):603-9.

122. Tumbarello DA, Kendrick-Jones J, Buss F. Myosin VI and its cargo adaptors - linking endocytosis and autophagy. J Cell Sci. 2013;126(Pt 12):2561-70.

123. Aschenbrenner L, Lee T, Hasson T. Myo6 facilitates the translocation of endocytic vesicles from cell peripheries. Mol Biol Cell. 2003;14(7):2728-43.

124. Aschenbrenner L, Naccache SN, Hasson T. Uncoated endocytic vesicles require the unconventional myosin, Myo6, for rapid transport through actin barriers. Mol Biol Cell. 2004;15(5):2253-63.

125. Naccache SN, Hasson T, Horowitz A. Binding of internalized receptors to the PDZ domain of GIPC/synectin recruits myosin VI to endocytic vesicles. Proc Natl Acad Sci U S A. 2006;103(34):12735-40.

126. Noguchi T, Frank DJ, Isaji M, Miller KG. Coiled-coil-mediated dimerization is not required for myosin VI to stabilize actin during spermatid individualization in Drosophila melanogaster. Mol Biol Cell. 2009;20(1):358-67.

127. Noguchi T, Lenartowska M, Miller KG. Myosin VI stabilizes an actin network during Drosophila spermatid individualization. Mol Biol Cell. 2006;17(6):2559-71.

128. Sakurai K, Hirata M, Yamaguchi H, Nakamura Y, Fukami K. Phospholipase Cdelta3 is a novel binding partner of myosin VI and functions as anchoring of myosin VI on plasma membrane. Adv Enzyme Regul. 2011;51(1):171-81.

129. Hertzano R, Shalit E, Rzadzinska AK, Dror AA, Song L, Ron U, et al. A Myo6 mutation destroys coordination between the myosin heads, revealing new functions of myosin VI in the stereocilia of mammalian inner ear hair cells. PLoS Genet. 2008;4(10):e1000207.

130. Avraham KB, Hasson T, Steel KP, Kingsley DM, Russell LB, Mooseker MS, et al. The mouse Snell's waltzer deafness gene encodes an unconventional myosin required for structural integrity of inner ear hair cells. Nat Genet. 1995;11(4):369-75.

131. Seiler C, Ben-David O, Sidi S, Hendrich O, Rusch A, Burnside B, et al. Myosin VI is required for structural integrity of the apical surface of sensory hair cells in zebrafish. Dev Biol. 2004;272(2):328-38.

132. Yoshida H, Cheng W, Hung J, Montell D, Geisbrecht E, Rosen D, et al. Lessons from border cell migration in the Drosophila ovary: A role for myosin VI in dissemination of human ovarian cancer. Proc Natl Acad Sci U S A. 2004;101(21):8144-9.

133. Dunn TA, Chen S, Faith DA, Hicks JL, Platz EA, Chen Y, et al. A novel role of myosin VI in human prostate cancer. Am J Pathol. 2006;169(5):1843-54.

134. Geisbrecht ER, Montell DJ. Myosin VI is required for E-cadherin-mediated border cell migration. Nat Cell Biol. 2002;4(8):616-20.

135. Finan D, Hartman MA, Spudich JA. Proteomics approach to study the functions of Drosophila myosin VI through identification of multiple cargo-binding proteins. Proc Natl Acad Sci U S A. 2011;108(14):5566-71.

136. Spudich G, Chibalina MV, Au JS, Arden SD, Buss F, Kendrick-Jones J. Myosin VI targeting to clathrin-coated structures and dimerization is mediated by binding to Disabled-2 and PtdIns(4,5)P2. Nat Cell Biol. 2007;9(2):176-83.

137. Yu C, Feng W, Wei Z, Miyanoiri Y, Wen W, Zhao Y, et al. Myosin VI undergoes cargo-mediated dimerization. Cell. 2009;138(3):537-48.

138. Lacroix E, Viguera AR, Serrano L. Elucidating the folding problem of alpha-helices: local motifs, long-range electrostatics, ionic-strength dependence and prediction of NMR parameters. J Mol Biol. 1998;284(1):173-91.

139. Kulic IM, Brown AE, Kim H, Kural C, Blehm B, Selvin PR, et al. The role of microtubule movement in bidirectional organelle transport. Proc Natl Acad Sci U S A. 2008;105(29):10011-6.

140. Kapitein LC, van Bergeijk P, Lipka J, Keijzer N, Wulf PS, Katrukha EA, et al. Myosin-V opposes microtubule-based cargo transport and drives directional motility on cortical actin. Curr Biol. 2013;23(9):828-34.

141. Kammerer S, Holzinger A, Welsch U, Roscher AA. Cloning and characterization of the gene encoding the human peroxisomal assembly protein Pex3p. FEBS Lett. 1998;429(1):53-60.

142. van Bergeijk P, Adrian M, Hoogenraad CC, Kapitein LC. Optogenetic control of organelle transport and positioning. Nature. 2015;518(7537):111-4.

143. Duan L, Che D, Zhang K, Ong Q, Guo S, Cui B. Optogenetic control of molecular motors and organelle distributions in cells. Chem Biol. 2015;22(5):671-82.

144. Townsley FM, Wilson DW, Pelham HR. Mutational analysis of the human KDEL receptor: distinct structural requirements for Golgi retention, ligand binding and retrograde transport. EMBO J. 1993;12(7):2821-9.

145. Scheel AA, Pelham HR. Identification of amino acids in the binding pocket of the human KDEL receptor. J Biol Chem. 1998;273(4):2467-72.

146. Kapitein LC, Schlager MA, van der Zwan WA, Wulf PS, Keijzer N, Hoogenraad CC. Probing intracellular motor protein activity using an inducible cargo trafficking assay. Biophys J. 2010;99(7):2143-52.

147. Schneider CA, Rasband WS, Eliceiri KW. NIH Image to ImageJ: 25 years of image analysis. Nat Methods. 2012;9(7):671-5.

148. Lister I, Schmitz S, Walker M, Trinick J, Buss F, Veigel C, et al. A monomeric myosin VI with a large working stroke. EMBO J. 2004;23(8):1729-38.

149. Morris CA, Wells AL, Yang Z, Chen LQ, Baldacchino CV, Sweeney HL. Calcium functionally uncouples the heads of myosin VI. J Biol Chem. 2003;278(26):23324-30.

150. Alexandre MT, Arents JC, van Grondelle R, Hellingwerf KJ, Kennis JT. A base-catalyzed mechanism for dark state recovery in the Avena sativa phototropin-1 LOV2 domain. Biochemistry. 2007;46(11):3129-37.

151. Pyrpassopoulos S, Feeser EA, Mazerik JN, Tyska MJ, Ostap EM. Membrane-bound myo1c powers asymmetric motility of actin filaments. Curr Biol. 2012;22(18):1688-92.

152. Yoshimura M, Homma K, Saito J, Inoue A, Ikebe R, Ikebe M. Dual regulation of mammalian myosin VI motor function. J Biol Chem. 2001;276(43):39600-7.

153. Furch M, Geeves MA, Manstein DJ. Modulation of actin affinity and actomyosin adenosine triphosphatase by charge changes in the myosin motor domain. Biochemistry. 1998;37(18):6317-26.

154. Llinas P, Pylypenko O, Isabet T, Mukherjea M, Sweeney HL, Houdusse AM. How myosin motors power cellular functions: an exciting journey from structure to function: based on a lecture delivered at the 34th FEBS Congress in Prague, Czech Republic, July 2009. FEBS J. 2012;279(4):551-62.

155. Le Roy C, Wrana JL. Clathrin- and non-clathrin-mediated endocytic regulation of cell signalling. Nat Rev Mol Cell Biol. 2005;6(2):112-26.

156. Wuytack F, Raeymaekers L, Missiaen L. PMR1/SPCA Ca2+ pumps and the role of the Golgi apparatus as a Ca2+ store. Pflugers Arch. 2003;446(2):148-53.

157. Li LH, Tian XR, Jiang Z, Zeng LW, He WF, Hu ZP. The Golgi Apparatus: Panel Point of Cytosolic Ca(2+) Regulation. Neurosignals. 2013;21(3-4):272-84.

158. Rock RS, Rief M, Mehta AD, Spudich JA. In vitro assays of processive myosin motors. Methods. 2000;22(4):373-81.

159. Meijering E, Dzyubachyk O, Smal I. Methods for cell and particle tracking. Methods Enzymol. 2012;504:183-200.

160. Nakamura M, Chen L, Howes SC, Schindler TD, Nogales E, Bryant Z. Remote control of myosin and kinesin motors using light-activated gearshifting. Nat Nanotechnol. 2014;9(9):693-7.

161. Altman D, Goswami D, Hasson T, Spudich JA, Mayor S. Precise positioning of myosin VI on endocytic vesicles in vivo. PLoS Biol. 2007;5(8):e210.

162. Tantama M, Martinez-Francois JR, Mongeon R, Yellen G. Imaging energy status in live cells with a fluorescent biosensor of the intracellular ATP-to-ADP ratio. Nat Commun. 2013;4:2550.

163. Russell JT. Imaging calcium signals in vivo: a powerful tool in physiology and pharmacology. Br J Pharmacol. 2011;163(8):1605-25.

164. Tantama M, Hung YP, Yellen G. Optogenetic reporters: Fluorescent protein-based genetically encoded indicators of signaling and metabolism in the brain. Prog Brain Res. 2012;196:235-63.

165. Christie JM, Corchnoy SB, Swartz TE, Hokenson M, Han IS, Briggs WR, et al. Steric interactions stabilize the signaling state of the LOV2 domain of phototropin 1. Biochemistry. 2007;46(32):9310-9.

166. Riedl J, Crevenna AH, Kessenbrock K, Yu JH, Neukirchen D, Bista M, et al. Lifeact: a versatile marker to visualize F-actin. Nat Methods. 2008;5(7):605-7.